Octupole collectivity in nuclei

P.A. Butler

Oliver Lodge Laboratory, Oxford St., University of Liverpool, Liverpool L69 7ZE, U.K.

E-mail: peter.butler@liverpool.ac.uk

March 2016

Abstract. The experimental and theoretical evidence for octupole collectivity in nuclei is reviewed. Recent theoretical advances, covering a wide spectrum from mean-field theory to algebraic and cluster approaches, are discussed. The status of experimental data on the behaviour of energy levels and electric dipole and electric octupole transition moments is reviewed. Finally, an outlook is given on future prospects for this field.

PACS numbers: 21.10.Re, 21.10.Ky, 23.20.Lv, 24.80.+y

Keywords: Nuclear Structure, Octupole Collectivity

1. Introduction

For the nuclear quantum system, spontaneous symmetry breaking that arises from deformation will in general lower its energy. This 'nuclear Jahn-Teller effect' [1] is illustrated by considering a simple nuclear Hamiltonian representing nuclear vibrations, written as (see [2] and references therein)

$$H = \sum_j e_j c_j^+ c_{j'} - \frac{1}{2} \sum_\lambda \kappa_\lambda \sum_{\mu=-\lambda}^{+\lambda} Q_{\lambda\mu}^+ \cdot Q_{\lambda\mu} + H_{\rm pair} \qquad (1)$$

In this expression the first term is the spherical shell-model potential, the second term represents the long-range multipole-multipole force generating the collective motion, and $H_{\rm pair}$ is the pairing Hamiltonian; j stands for the set of quantum numbers (n, ℓ, j). Spherical symmetry will be removed for $\lambda = 2$ quadrupole-quadrupole interactions, and most nuclei are quadrupole deformed in their lowest energy state. For some combinations of Z and N the nucleus can further lower its energy through octupole-octupole interactions, and the nucleus no longer retains reflection symmetry . In a mean-field description of the nucleus, octupole correlations depend on the matrix elements of the spherical harmonic Y_3^0 between single particle states with $\Delta j = \Delta \ell = 3$ and the spacing between them. The left hand side of figure 1 shows that the proton number

and neutron numbers, where such states approach the Fermi surface and the spacing is small, are $\approx 34, 56, 88, 134$, that is, at values just greater than the magic numbers where nuclei are nearly spherical. These values are superimposed on the chart of nuclides in the right hand side of figure 1; it is apparent that regions of largest octupole correlations occur for the β^--decaying neutron-rich nuclei to the north east of ^{132}Sn or for the mostly α-decaying nuclei north-east of ^{208}Pb.

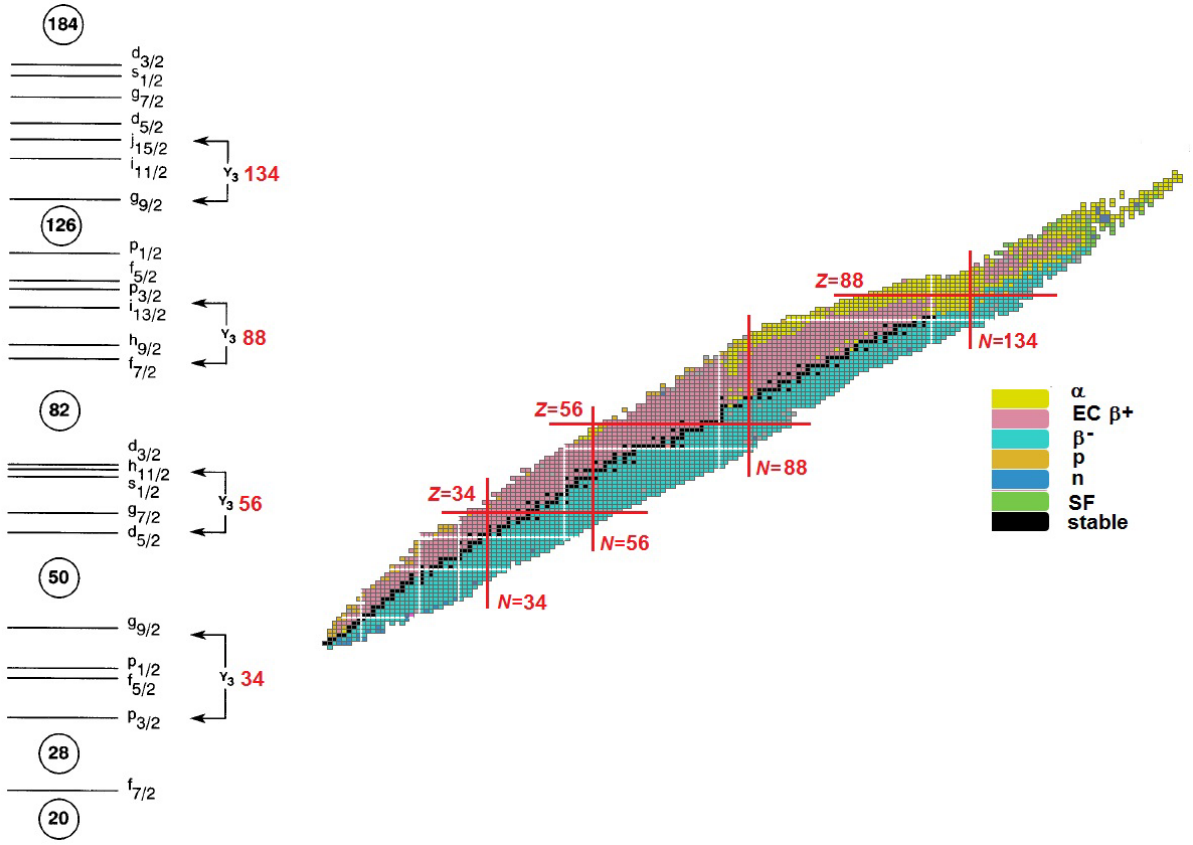

Figure 1: Left hand side: nuclear spherical single-particle levels. The most important octupole couplings are indicated. Right hand side: chart of nuclides for which the proton and neutron numbers having the strongest octupole coupling are indicated. The white lines indicate the positions of the magic numbers. The modes of radioactive decay are given in the legend; stable isotopes are in black.

In order to visualise reflection-asymmetric nuclei it is convenient to consider the generalised Rayleigh shape of a macroscopic object where its surface is given by in terms of a spherical harmonic (multipole) expansion

$$R(\Omega) = c(\alpha)\left[1 + \sum_{\lambda=2}^{\infty}\sum_{\mu=-\lambda}^{+\lambda} \alpha_{\lambda\mu} Y^*_{\lambda\mu}(\Omega)\right] \tag{2}$$

In this expression $c(\alpha)$ is determined from the volume-conservation condition and $R_0 = r_0 A^{\frac{1}{3}}$. The standard deformation parameters $\alpha_{\lambda\mu}$ can be reduced in number by imposing the centre of mass to be the same as the origin of the body-fixed frame and assuming that the shape has axial symmetry, giving

$$\beta_\lambda = \alpha_{\lambda 0}, \quad \lambda = 2, 3, 4, ... \tag{3}$$

All other values of $\alpha_{\lambda\mu}$ are zero. For a nucleus the charge and mass distribution can be approximated by this expansion and shape parameterisation in terms of β_λ is a convenient starting point for mean field calculations. A graphical representation of the shapes of octupole-deformed nuclei are given in figure 2, where the values of β_2, β_3 and β_4 are taken from an analysis of octupole instability in nuclei using Strutinsky-type potential-energy calculations [3]. The example on the left hand side of figure 2, ^{220}Rn, is supposed to have an octupole instability, i.e there is an octupole vibration around $\beta_3 = 0$ whereas ^{224}Ra on the right-hand side is supposed to be an example of permanent octupole deformation (see figure 3), $\beta_3 \neq 0$.

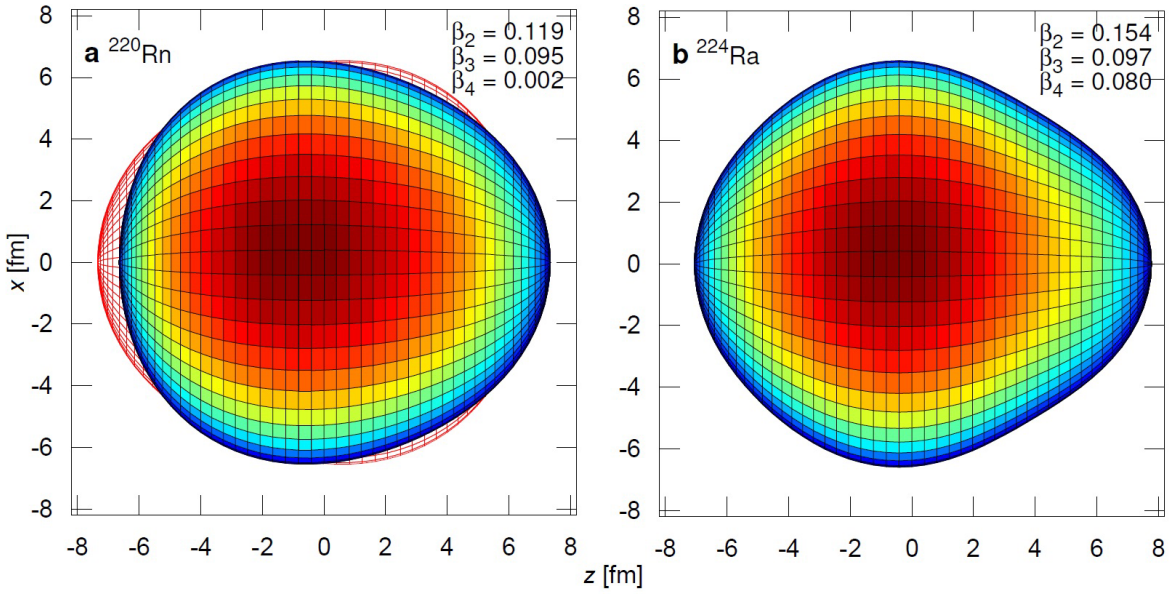

Figure 2: Graphical representation of the shapes of ^{220}Rn and ^{224}Ra, taken from [4]. **a**, ^{220}Rn; **b**, ^{224}Ra. Panel **a** depicts vibrational motion about symmetry between the surface shown and the red outline, whereas **b** depicts static deformation in the intrinsic frame. Theoretical values of β_4 are taken from ref. [3]. The colour scale, blue to red, represents the y-values of the surface. The nuclear shape does not change under rotation about the z axis.

As stated earlier strong octupole correlations leading to pear shapes can arise for certain proton and neutron numbers Z and N. When both proton and neutron numbers have these values, such as for $Z \sim 56$, $N \sim 88$ and $Z \sim 88$, $N \sim 134$ we expect the best evidence for reflection asymmetry. The bulk of the evidence comes from the behaviour of energy levels for even-even nuclei. If such nuclei are reflection-symmetric,

the intrinsic system is invariant under both the parity ($\mathcal{P}$) operation and rotation of the system through π about an axis perpendicular to the symmetry axis ($\mathcal{R}$), giving rise to laboratory projections of the angular momentum and parity for the rotating system of $I^\pi = 0^+, 2^+, 4^+, ...$ If the potential barrier under octupole deformation β_3 reaches a minimum for $\beta_3 = 0$ then the nucleus is on average reflection symmetric but undergoes oscillations around $\beta_3 = 0$ (see figure 3a); the associated phonon has $L = 3\hbar$. If the z-axis is the body-fixed symmetry axis and the nucleus rotates about the x-axis, then the rotational-vibrational bands will have $K^\pi = 0^-, 1^-, 2^-, 3^-$ where $K = \boldsymbol{L}_z$ is the constant projection on the z-axis. In general, as pointed out by Neergård and Vogel [5] using the framework of the random-phase approximation, for the lightest actinide and rare-earth nuclei the $K^\pi = 0^-$ bandheads come lowest, while for the heavier ones the $K^\pi = 2^-$ and $K^\pi = 1^-$ bandheads share the lowest position.

For reflection-asymmetric nuclei, the intrinsic system is only invariant under the product $\mathcal{RP}$, so that [6]

$$\sigma = 0,\ I^\pi = 0^+, 1^-, 2^+, 3^-, 4^+, ...$$
$$\sigma = 1,\ I^\pi = 0^-, 1^+, 2^-, 3^+, 4^-, ...$$

In these expressions σ is the simplex, defined so that the eigenvalue of $\mathcal{I} = \mathcal{P}.\mathcal{R}^{-1}$ is $e^{-i\sigma\pi}$ [7]. $\mathcal{I}$ is the operator that reflects in a plane containing the symmetry axis. (For a full description of possible symmetries see the review by Frauendorf [7].) For real nuclei the low-lying negative parity states in the $\sigma = 0$ band are pushed higher in energy relative to the positive-parity states, while the negative-parity band has a larger moment of inertia at low spin compared to the positive-parity band (see figure 3b). The displacement of the negative-parity band relative to the ground state band near the ground state is associated with the lowering of the barrier at $\beta_3 = 0$ between the reflection-asymmetric shapes, which is a consequence of pairing at low spin for even-even nuclei. This also accounts for the elevated excitation of the $\sigma = 1$ band relative to the $\sigma = 0$ band.

For odd-mass nuclei, the odd proton or neutron has angular momentum $\boldsymbol{j}$ so that the total angular momentum $\boldsymbol{I}$ has projection $K = \boldsymbol{j}_z$ on the z-axis. In this case there will be two $K^\pm$ bands of differing simplex:

$$\sigma = +1/2,\ I^\pi = K, (K+1), (K+2), (K+3), ...\ \pi = (-)^{I-\frac{1}{2}}$$
$$\sigma = -1/2,\ I^\pi = K, (K+1), (K+2), (K+3), ...\ \pi = (-)^{I+\frac{1}{2}}$$

Because of the reduction in pairing for odd-A nuclei, the two simplex bands are expected to lie close in energy giving rise to a parity doublet (see figure 3c).

The underlying theoretical evidence for reflection asymmetry in nuclei, and the experimental evidence for strong octupole correlations, such as interleaved positive- and negative-parity rotational bands in even-even nuclei and parity doublets in odd-mass nuclei has been given in two broad overviews [10, 2]. These reviews also look at the available evidence from electromagnetic transition rates, particularly enhanced electric dipole ($E1$) and octupole ($E3$) transitions, and spectroscopic properties of the

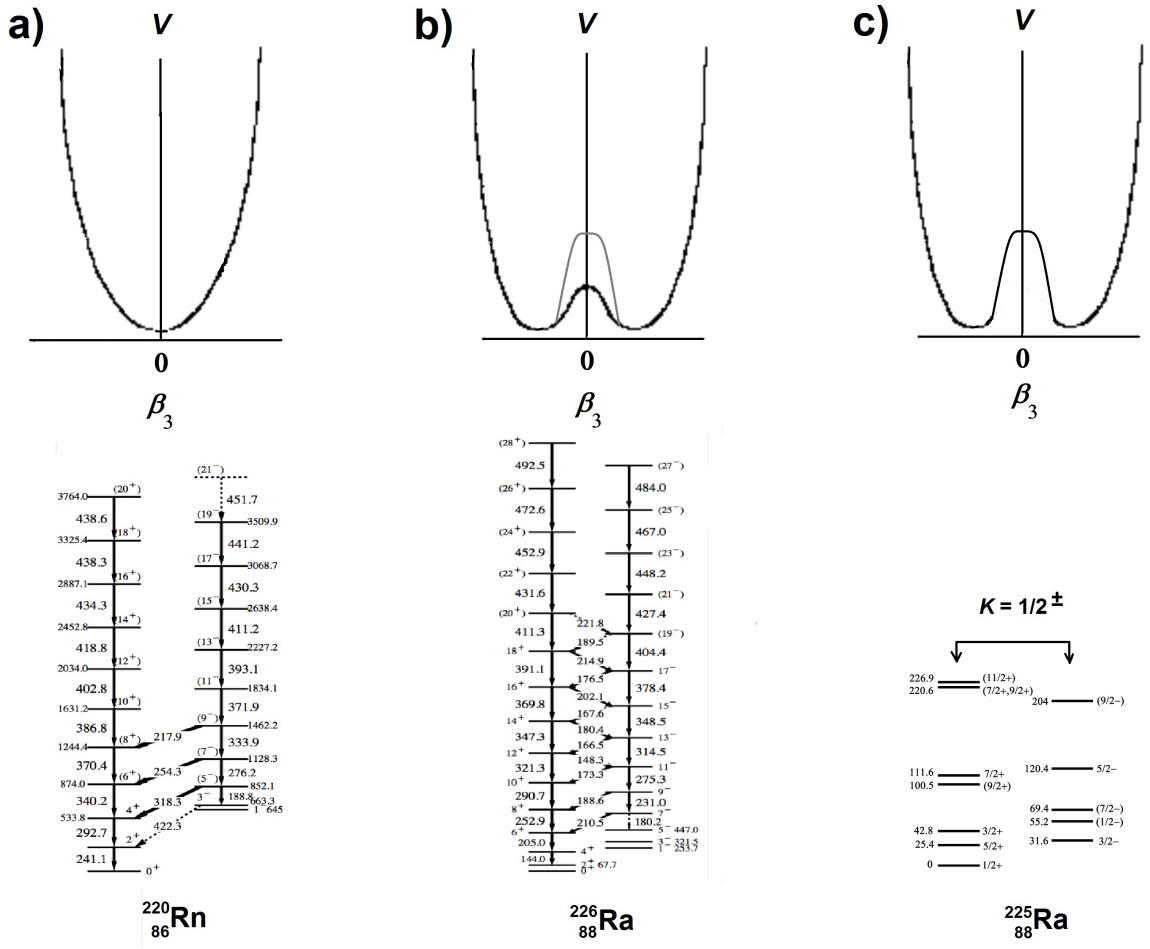

Figure 3: Nuclear potential energy as a function of octupole deformation β_3 for an octupole vibrator (a) and a system having permanent octupole deformation (b,c). For nuclei having permanent octupole deformation, the barrier increases with angular momentum as pairing is reduced. Figure (c) represents a nucleus where the barrier is high in the ground state, which would be the case for odd-A. The three cases (a), (b) and (c) are illustrated by actual nuclei ^{220}Rn [8], ^{226}Ra [8] and ^{225}Ra(adapted from [9]). For the last case, the decoupling parameters a for the $K = \frac{1}{2}^+$ and $K = \frac{1}{2}^-$ bands have opposite sign [11, 12].

odd particle in odd-A nuclei. A comprehensive discussion of the latter can be found in [11, 12]. This review will focus on selected recent theoretical approaches (section 2), experimental data on energy levels (section 3) and electromagnetic transition rates, particularly $B(E3)$s (section 4). The final section(5) will look at future prospects for this field.

2. Recent theoretical approaches

Many theoretical approaches have been developed to describe the observed experimental features. Some of these have been reviewed previously [2] such as macroscopic (liquid-drop) - microscopic (shell-corrected) models [3, 13], microscopic mean-field or many-body approaches using various interactions [14, 15, 16, 17, 18, 19, 20], models that assume α-particle clustering in the nucleus [21, 22], and algebraic models [23].

Following the early work of Bonche *et al.*, who carried out self-consistent Hartree-Fock + BCS (HFB) quadrupole-octupole calculations for the ground state of ^{222}Ra using the Skyrme III effective interaction [15], Tsvetkov *et al.* [24] applied a similar approach to analyse the rotational dependence of the quadrupole and octupole moments in Ra, Th and U isotopes. They also calculated, with mixed success, the electric dipole moments Q_1 in these isotopes. Calculations of octupole deformation β_3 and Q_1 were carried out by Engel, Dobaczewski and co-workers [18] using a variety of Skyrme interactions. They also calculated intrinsic Schiff moments, relevant to the study of CP-violating static EDM moments (see section 5).

Egido and Robledo [16] used the HF+BCS as well as beyond the mean-field approaches, using the Gogny interaction, to study the octupole degree of freedom in Ra and Th isotopes. More recently, Robledo and Bertsch [20] performed a systematic study of octupole excitations (including $B(E3, 3^- \rightarrow 0^+)$ values) in even-even nuclei using the generator-coordinate extension (GCM) of the HFB self-consistent mean field theory, using the Gogny family of Hamiltonians. Examples of such calculations are given in figure 4. Although the theory reproduces the overall trend of the excitations including the effects of static octupole deformation and the most visible shell effects, the authors point out that the overall scaling factor of 1.6 could arise from deficiencies in the Gogny interaction or from the restriction of the degrees of freedom in the excitation to a single variable. These calculations have been extended to soft deformed nuclei [25] and heavy actinide nuclei [26]. A two-dimensional GCM calculation to deal with the quadrupole-octupole coupling for Rn, Ra and Th isotopes has improved the agreement for excitation energies and $B(E3)$ values for these nuclei [27].

A systematic analysis of low-lying quadrupole and octupole collective states, based on the relativistic energy density functional (EDF) has been made for actinide and rare-earth nuclei [28]. In these relativistic Hartree-Bogoliubov (RHB) calculations, the deformation constrained self-consistent axially-symmetric mean-field energy surfaces were mapped onto the equivalent Hamiltonian of the *sdf* interacting boson model (IBM), allowing the IBM Hamiltonian generate the excitation spectra and electromagnetic transition rates. In the actinide region the RHB calculations predict stable octupole deformation for $^{222-226}$Ra and $^{224-228}$Th, while in the rare-earths $^{144-146}$Ba and ^{150}Sm have pronounced octupole mimima. The calculations for rare-earth nuclei have been repeated using the Gogny force, again mapped onto a IBM *sdf* Hamiltonian. It is interesting to note that the Gogny-EDF calculations predict a much shallower octupole minimum for ^{150}Sm. A discussion of the comparison with experimental electric transition

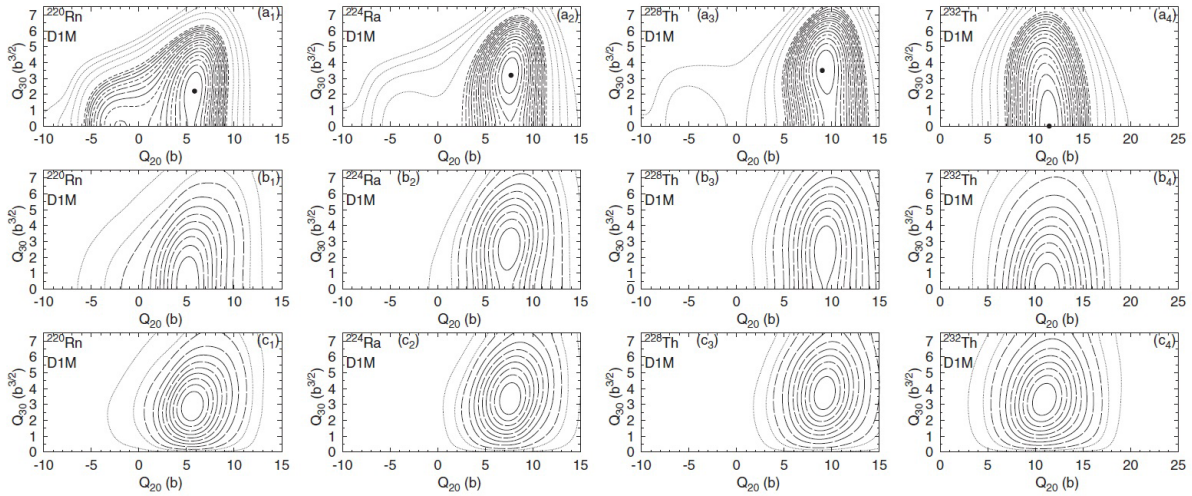

Figure 4: Upper row (a_1 to a_4): contour plots of the HFB energy surfaces as a function of the axially symmetric shape operators $Q_{\lambda 0}$ obtained with the Gogny D1M interaction, depicted for several Ra and Th isotopes. The position of the ground state minimum is indicated by a bullet. In the middle row (b_1 to b_4) the ground state collective amplitudes are shown. In the bottom row (c_1 to c_4), the corresponding amplitudes for the first negative parity excited state are given. For further details see [27].

strengths is left for section 4, but has been noted by the authors reproduction of the experimental behaviour of $B(E1)$ strengths remains a challenge.

Several authors have speculated, based on group-theoretical considerations and calculations using several types of mean-field method (see, for example [29, 24, 30, 31, 32, 33]) that nuclei can assume tetrahedral shapes, for which $\alpha_{32} \neq 0$ (see equation 2), that break the symmetry by inversion. In the ideal case of pure tetrahedral symmetry with no other multipole deformations present, the $E1$ and electric quadrupole ($E2$) moments are expected to be zero and the first nonvanishing moments will have $\lambda = 3$. In such a case, there will be parity-doublet bands with degenerate sequences $0^+, 1^-, 2^+, 3^-, ...$ and $0^-, 1^+, 2^-, 3^+, ...$ connected by pure $E3$ transitions rather than $E2$ or $E1$ transitions. As yet, searches for evidence of tetrahedral shapes in nuclei have proved unsuccessful [34, 35, 36].

The failure of collective models of rotating pear-shapes to account for the excitation energies of the negative parity states relative to the positive parity states has been addressed by Frauendorf [38]. He points out that the two bands of different parity do not merge for some nuclei (e.g. ^{220}Ra) at higher spin but instead cross. This is unexpected if the shift of the negative-parity states relative to the positive-parity states at low spin arises from tunneling between the two pear shapes, where the barrier at $\beta_3 = 0$ is reduced because of pairing. He suggested instead that the excitation arised from the condensation of rotational-aligned octupole phonons.The state with maximal angular momentum for given energy (yrast state) is generated by aligning the angular momenta of all bosons with the axis of rotation. The total angular momentum and the

energy of the aligned n-boson state are, respectively, given by

$$I = ni + \omega\mathcal{J}$$
$$E_n(I) = \hbar\Omega_3(n + \frac{1}{2}) + \frac{(I - ni)^2}{2\mathcal{J}}$$

where each boson carries $i \approx 3\hbar$ of angular momentum. In these expressions Ω_3 is the frequency of the octupole vibration and $\mathcal{J}$ is the moment of inertia of the quadrupole deformed nucleus assumed to be a rigid rotor. The inclusion of anharmonicities in the octupole vibration tend to synchronize the rotation of the condensate and the quadrupole shape of the nucleus forming a rotating heart shape. This model has been used to interpret the behaviour of the energy levels in even-even Ra and Th isotopes [37, 38], and more recently in ^{240}Pu [39] (see section 3).

Minkov and collaborators have proposed a collective model formalism which describes both the parity shift observed in low-lying spectra and the fine rotational band structure developed at higher-angular momenta, as arising from the interplay between the octupole shape oscillation (parity shift) mode and the stable quadrupole-octupole rotation mode. Using this formalism they obtained good agreement between the theoretical and experimental levels with a standard root mean square deviation of less than 20 keV for ^{224,226}Ra and ^{224,226}Th [40]. Similar methods have been applied to explain the high-spin behaviour of ^{220}Ra [41] (see section 3) and ^{144,146}Ba [42].

The deformed shell model in which pairing is taken into account using the BCS procedure has been applied to the study of high-K isomers in heavy actinide, transfermium and rare-earth nuclei [43, 44, 45]. The results of the calculations indicate regions of nuclei with octupole softness as well as possible octupole deformation in the high-K isomeric states. The best examples where octupole deformation might occur include the $K^\pi = 6^-$ isomer in ^{234}U and the $K^\pi = 8^-$ isomer in ^{254}No [45]. Similar results are reported in [46].

An interesting approach to the octupole degree of freedom has been made by Bizzeti and Bizzeti-Sona who have made an analysis in terms of the $X(5)$ phase transition between spherical and deformed axially symmetric shape [47], using a geometrical parametrization of the nuclear shape. They found [48] that ^{226}Th lies close to the critical point of the phase transition between harmonic octupole oscillation and a permanent asymmetric shape. More recent calculations have been made for energy levels and transition strengths in the transitional nuclei ^{224,226}Ra and ^{224}Th [49, 50], ^{150}Nd and ^{152}Sm [51].

In contrast to the concept of a mean field which has a dynamic or static octupole deformation, another approach is to assume that the reflection-asymmetric shape is a consequence of the addition of dipole and/or octupole bosons in the IBM model. Zamfir and Kusnezov have studied the properties of even-even Ra-Th nuclei in the framework of the *spdf* interacting boson model [23]. The $f(L^\pi = 3^-)$ boson had been introduced earlier to describe octupole vibrations in quadrupole-deformed nuclei [52]. In order to describe the low-lying $K^\pi = 0^-$ bands in transitional actinides, p ($L^\pi = 1^-$) bosons have to be introduced, as demonstrated by Otsuka and Sugita [53]. The more recent

calculations [23] show that the addition of one pf boson is sufficient to reproduce the essential features of the alternating parity bands in the light actinides, at least at low spin. However, the observed zero-crossing of the value of Q_1 for ^{224}Ra (see section 4; the authors actually calculated $B(E1)/B(E2)$ ratios) could only be reproduced by introducing large A-dependence for the $E1$ effective charge.

The IBM approach is related to alpha clustering in nuclei (see e.g. [54, 23]), or a cluster configuration with a lighter cluster heavier than ^{4}He (see e.g. [22]). Shneidman *et al.* have carried out detailed surveys of rare-earth and actinide nuclei using a Hamiltonian for dinuclear systems first introduced to explain heavy-ion reaction data [21]. The light mass in these calculations is restricted to Li and α-clusters. The calculations are able to reproduce experimental data on the angular momentum dependence of parity splitting of the energy levels, although as will be seen in section 4 the predictions for $B(E\lambda)$ transition rates have mixed success.

3. Energy levels

The observation [55], 60 years ago, of a low-lying 1^- state in ^{224}Ra populated by α-decay led almost immediately to the suggestion (see ref. [56] for reference) that "this state may have the same intrinsic structure as the ground state and represents a collective distortion in which the nucleus is pear-shaped." The energy of this 1^- state, while being the lowest observed of all nuclei, lies higher than that of the 2^+ member of the ground state rotational band. The level scheme of ^{224}Ra obtained by the α-decay studies is shown in the left-hand side of figure 5.

Experiments to extend both positive and negative parity bands to higher spins using nuclear reactions were carried out much later. Information on the high-spin behaviour of energy levels and $B(E1)/B(E2)$ branching ratios nuclei in the actinide region (including $Z = 86 - 89$ in this definition) from nuclear reaction studies usually required advanced experimental techniques to remove the background from the dominant fission background. For exploiting compound nucleus reactions, evaporation residual detectors in conjunction with γ-ray arrays and conversion electron spectrometers have been used to study ^{222}Th [57], ^{220}Ra [58], ^{223}Th [59] with $\approx$ 1mb cross-sections or recoil-decay tagging methods for ^{226}U [60, 61] where the cross-section is $\approx 1\mu$b. Coulomb excitation (Coulex) of radioactive ($t_{\frac{1}{2}} = 1600$ year) ^{226}Ra targets provided extensive data on energy levels and electromagnetic moments [62] (see section 4) while the use of heavy-ion transfer reactions on ^{226}Ra provided high-spin data on ^{224}Ra [63]. The advent of highly efficient γ-ray arrays enabled ^{220}Ra and ^{222}Th be measured at high spin without the requirement for evaporation recoil detectors [64], and allowed the level schemes of several Rn, Ra and Th isotopes, populated as products of deep-inelastic scattering [65] of the ^{136}Xe+^{232}Th reaction, to be extended to high spin [66, 8]. The level scheme of ^{224}Ra obtained in this manner [66] is shown in the right-hand side of figure 5. In the lanthanide region (including $Z = 54 - 57$ in this definition) some of the nuclei expected to have strong octupole correlations are stable and have been studied

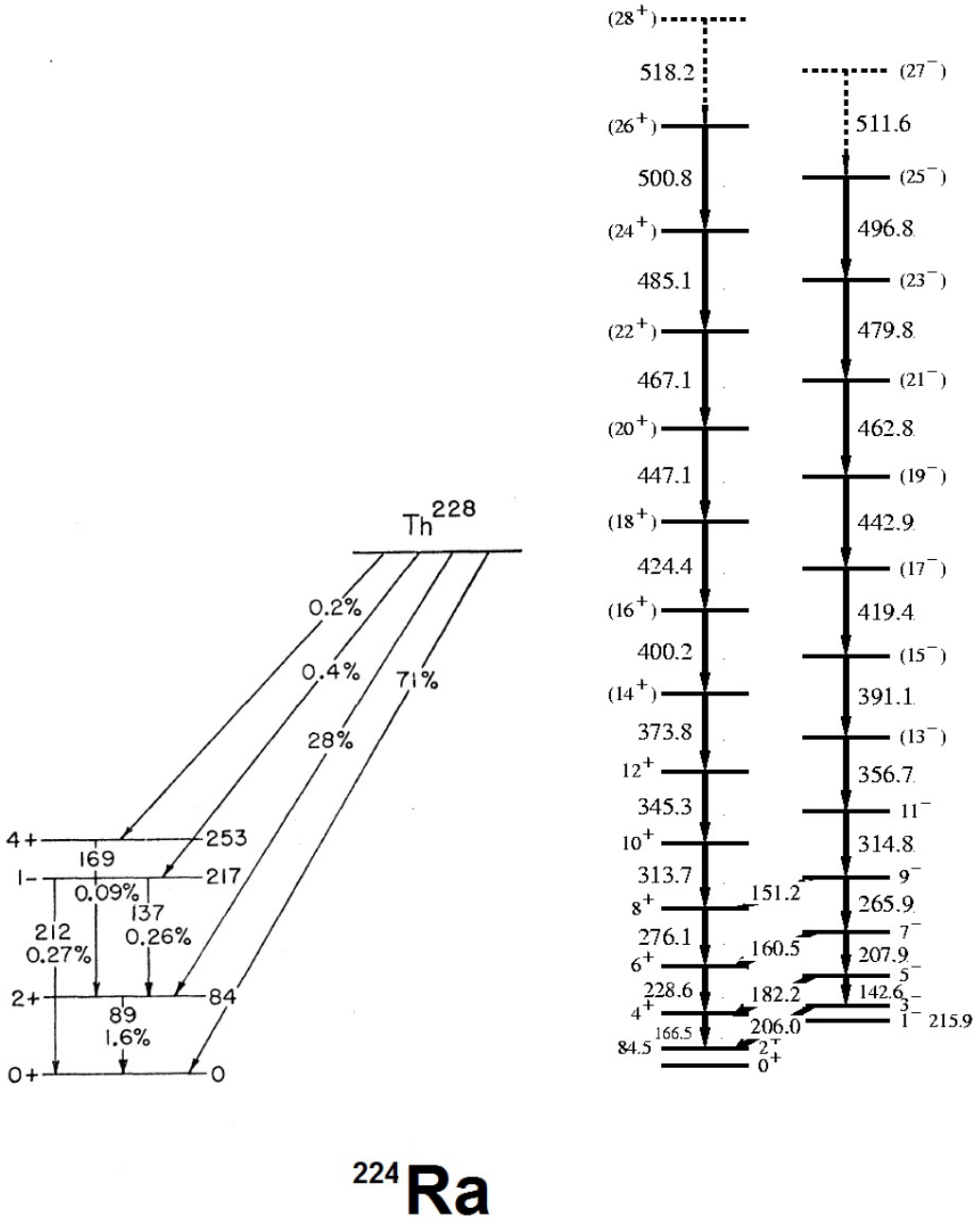

Figure 5: Left-hand side: level scheme of ^{224}Ra obtained from α-decay studies [55]. Right-hand side: extended scheme obtained from in-beam γ-ray measurements [8].

using Coulomb excitation [67, 68, 69] but most information has exploited spontaneous fission-fragment γ-ray spectroscopy following the pioneering experiments of Phillips and collaborators [70] (see also [71]). This method has been reviewed in [72]. Figure 6 shows regions of the chart of nuclei for which high-spin data are available, obtained using the

various reactions discussed above.

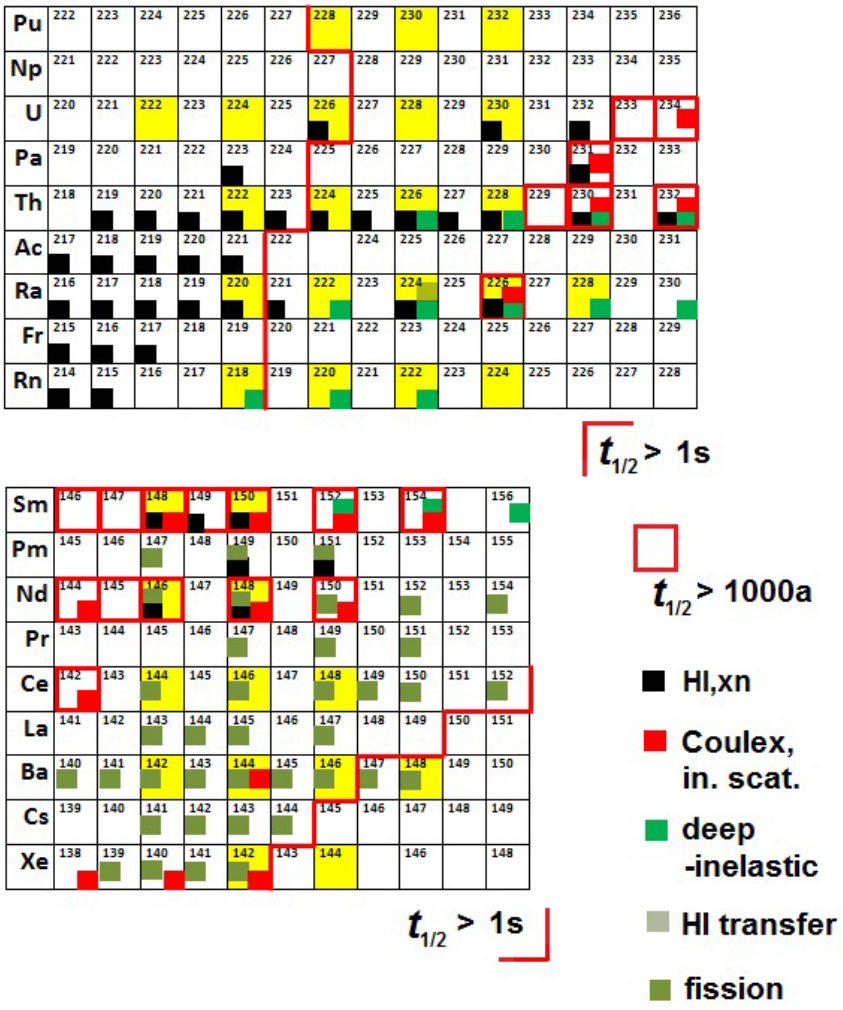

Figure 6: Nuclei studied at high spin using heavy-ion induced CN reactions (mostly through xn channels), Coulomb excitation (or inelastic scattering), deep-inelastic reactions, heavy-ion transfer reactions, or spontaneous fission. Isotopes with sufficiently long half-lives ($>$ 1000 years) to make targets are outlined. The even-even nuclides highlighted in yellow are those predicted to have a minimum potential energy for non-zero β_3 [20, 25]. Upper: nuclei with $Z \approx 88$, $N \approx 134$. Highlighted is the boundary at which nuclei with more neutrons have half-lives sufficient ($>$ 1s) for post-acceleration. Lower: nuclei with $Z \approx 56$, $N \approx 88$. Highlighted is the boundary at which nuclei with less neutrons have half-lives sufficient ($>$ 1s) for post-acceleration.

One of the most important indicators of whether a nucleus is reflection-asymmetric or not is the behaviour of the energy levels themselves. Alternating negative and positive parity states can arise in a number of ways from instability in the octupole degree of

freedom, see figure 3. One limit is that the nucleus has permanent octupole deformation, in which case the component of angular momentum aligned to the rotation axis of a state having positive parity, i_x^+, or negative parity, i_x^-, is equal to the rotational angular momentum, R. In this case the difference in aligned angular momentum, $\Delta i_x = i_x^- - i_x^+$, at the same rotational frequency ω, is equal to zero. The other limit is that the negative parity band arises from octupole vibrations of the rotating (quadrupole) deformed system. Here the negative parity states are formed by coupling $\boldsymbol{R}$ to the angular momentum of the octupole phonon ($3\hbar$). If the phonon angular momentum is aligned to $\boldsymbol{R}$ then $\Delta i_x = 3\hbar$ for a given value of ω. If the lowest negative parity band has $K^\pi = 0^-$ (and this seems to provide the most favourable situation for alignment of the phonon) then the resulting spectrum can give rise to an alternating sequence of negative and positive parity states. Plots of Δi_x versus $\hbar\omega$ for nuclei in the $Z \approx 88$, $N \approx 134$ mass region are given in figure 7. As can be seen, there are several examples such as ^{222,224,226}Ra and ^{224,226}Th where the value of Δi_x tends to zero for $\hbar\omega > 0.15$MeV. The Rn isotopes, with A=218-222, on the other hand, are almost perfect octupole vibrators [66, 8]. In ^{226}U the behaviour of Δi_x as a function of $\hbar\omega$ is

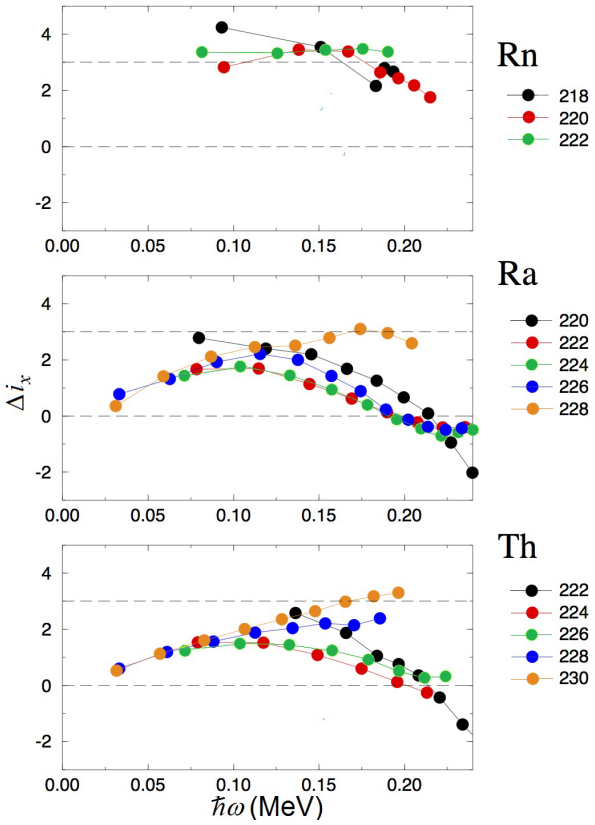

Figure 7: Plot of the difference in aligned angular momentum, $\Delta i_x = i_x^- - i_x^+$ against rotational frequency for isotopes of Rn, Ra and Th. Adapted from [8].

almost identical to that of its isotones ^{222}Ra, ^{224}Th and approaches 0 at $\hbar\omega \sim 0.2$MeV,

contrasting to the behaviour of ^{220}Rn, see figure 8 [60].

In ^{220}Ra the alternating-parity states have been observed up to $I \sim 30\hbar$ while the corresponding level structure in ^{222}Th appears to terminate at significantly lower spin [64]. These observations are consistent with Woods-Saxon-Bogolyubov cranking calculations [73] which predict that the yrast band of Th will undergo a shape transition at $I = 24\hbar$, in contrast to that of Ra which maintains its reflection asymmetry to higher spins. In contrast, $^{238-240}$Pu are found to exhibit properties associated with stable octupole deformation at the highest spins, suggesting that a transition with spin from a vibration to stable deformation may have occurred [74].

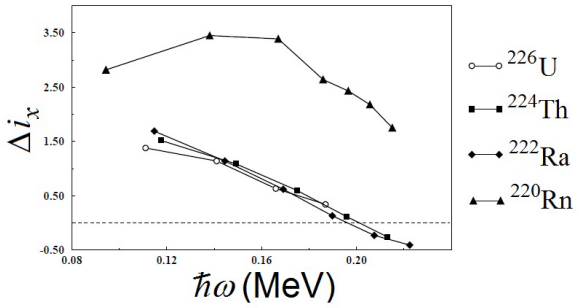

Figure 8: Plot of the difference in aligned angular momentum, $\Delta i_x = i_x^- - i_x^+$ against rotational frequency for the $N = 134$ isotones, $Z = 86 - 92$. Taken from [60].

In the $Z \approx 56$, $N \approx 88$ mass region, see figure 9, most nuclei in this mass region behave like octupole vibrators. For three examples, ^{148}Ce, ^{150}Nd, and ^{152}Sm, the value of Δi_x is significantly smaller than $3\hbar$ near the ground state and cross zero at around $\hbar\omega \sim 0.25$MeV. For these $N = 90$ nuclei the low-lying collective negative-parity bands cross bands built on particle-hole excitations that are well described by the Cranked Shell Model [75]. For the $N = 86$ nuclei ^{144}Ba, ^{146}Ce, ^{148}Nd and ^{150}Sm, HFB calculations [76] predict a phase transition from octupole vibrational to octupole deformation as I approaches $10\hbar$.

As discussed earlier, a more sophisticated description of octupole vibrations interprets the observed strong octupole correlations as a rotation-induced condensation of octupole phonons having their angular momentum aligned to the rotation axis. In this model the bands arising from multi-phonon alignment, where n, the number of phonons, has values $1, 2, 3, ...$ cross at the same critical frequency. Deviations from the idealised scenario of harmonic, noninteracting bosons will delay the crossing for the bands of higher n. This description has been tested for ^{240}Pu, where it has been possible to carry out a high-statistics experiment using inelastic scattering of heavy ions ('unsafe' Coulomb excitation) [39]. Figure 10 shows the measured alignment of respectively the ground-state positive parity band (band 1), the lowest octupole negative-parity band (band 2) and the lowest excited positive-parity band based on a $K^\pi = 0^+$ bandhead

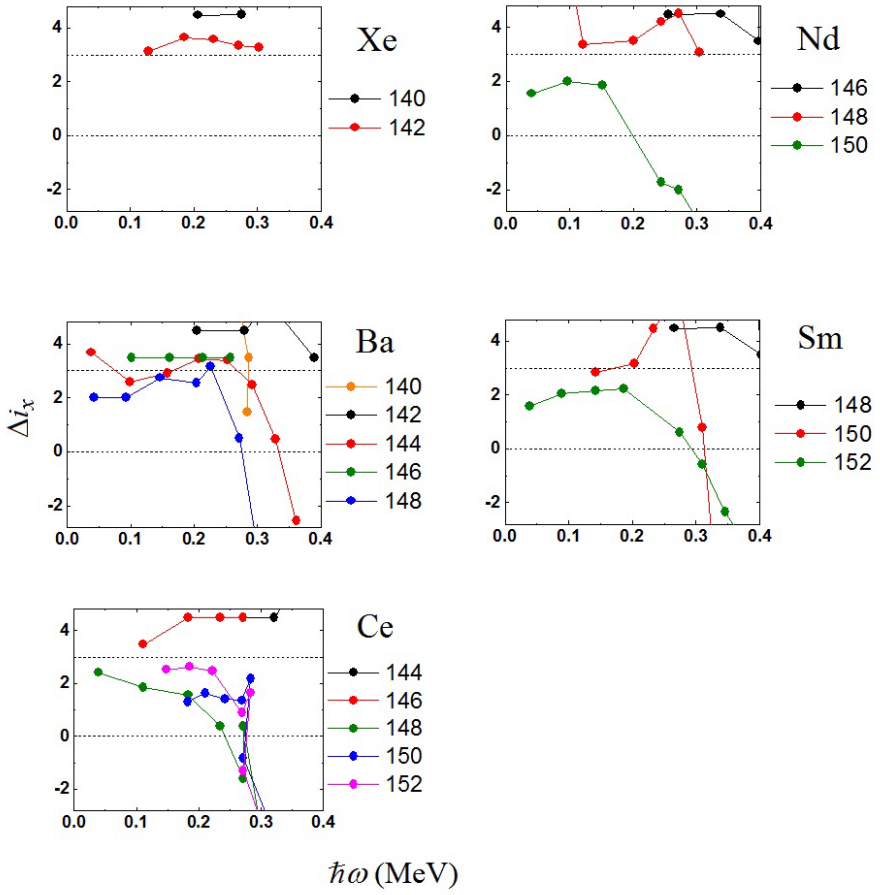

Figure 9: Plot of the difference in aligned angular momentum, $\Delta i_x = i_x^- - i_x^+$ against rotational frequency for isotopes of Xe, Ba, Ce, Nd and Sm. The data are taken from [2] (references therein) and [77, 78, 79, 80, 81, 82, 83].

at $E_x = 861$ keV (band 3). The bands are interpreted as $n = 0$ (band 1), $n = 1$ (band 2) and $n = 2$ (band 3) phonon bands, with respective i_x values of approximately 0, 3 and $6\hbar$ resulting from the alignment of the octupole phonons with the rotation axis. This interpretation provides a natural explanation for the sole presence of $E1$ transitions between bands 3 and 2 as only transitions between states differing by a single phonon are allowed within such a vibrational picture. This behaviour has also been observed in ^{238}U [84]. Excited 0^+ states in ^{240}Pu have been studied recently using the (p,t) reaction, and the application of the *spdf*-interacting boson model to interpret these states supports the proposed octupole correlations in the structure of the $K^\pi = 0_2^+$ band [85]. It should be noted that similar behaviour for the $E1$ decay of excited $K^\pi = 0^+$ bands, that only proceeds to the octupole band and not to the positive-parity ground-state band, has been observed in ^{226}Ra [86] and ^{228}Th [87]. The behaviour of $E3$ transitions within vibrational bands will be further discussed in sections 4 and 5.

We have seen that the rotational spectra of odd-A nuclei where the odd nucleon is

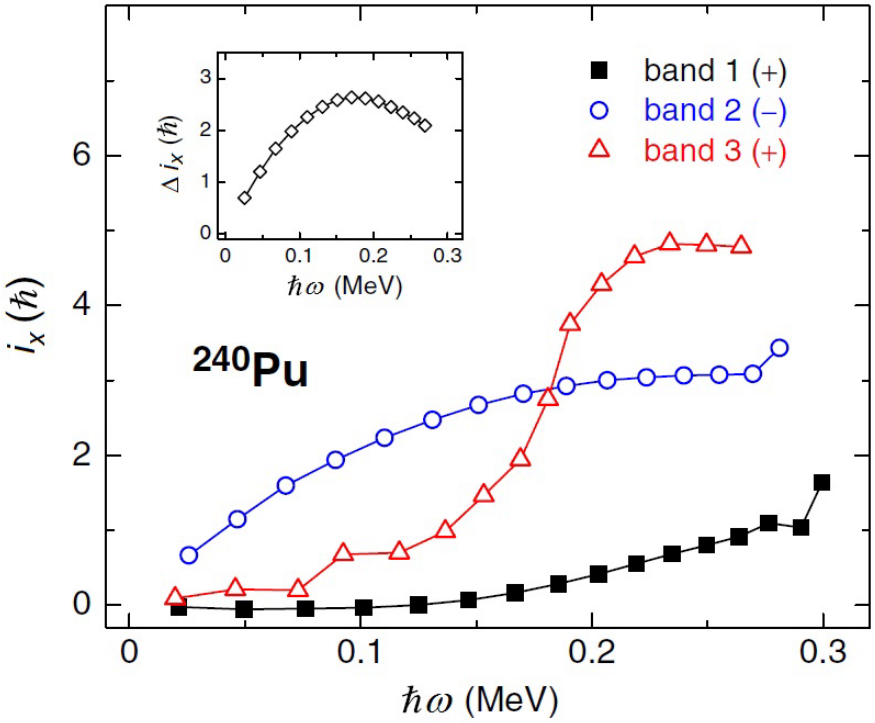

Figure 10: Aligned spins i_x as a function of rotational frequency deduced for bands 1, 2, and 3 in ^{240}Pu. The inset provides the relative alignment Δi_x of band 2 with respect to the yrast sequence. Bands 1, 2 and 3 are the ground state band, lowest negative parity band, and positive parity band built upon the $K = 0_2^+$ bandhead. See [39] for details.

coupled to a rigid reflection-asymmetric even-even core will have parity-doublet bands where the states having the same spin but opposite parity will be degenerate in energy. Most of the spectroscopic data on the low-lying states in heavy nuclei, that revealed evidence for octupole distortions, arose from α- or β-decay studies. For even-even nuclei populated by α-decay, the near-perfect alignment of the excited states in the daughter nucleus allows the final spins and parities to be assigned even for the weakly populated negative parity states using α-γ correlations (see, e.g. [88, 89]). A much larger spectrum of states is populated by β-decay of exotic nuclei produced, for example, by proton spallation of thorium or uranium, which has provided much of the data on odd$-A$ heavy nuclei. An example of this is the detailed study of low-lying states in ^{229}Ra [90] where γ-ray, internal conversion electron, and lifetime measurements were carried out. In contrast, α-decay studies have so far failed to identify the low-lying negative state partners of the ground-state $K^\pi = 5/2^+$ band in ^{223}Th [91, 92]. A compilation of the properties of odd-mass (and odd-odd) nuclei is given in reference [2], which identifies several nuclei with $Z \approx 88$, $N \approx 134$ where the ground state and its simplex partner are separated by an energy that is less than 70keV: ^{223}Ra, ^{225}Ra,^{223}Ac, ^{225}Ac, ^{227}Ac and

^{227}Th. Subsequent investigations have reinforced the findings for ^{227}Th [93, 94] while the results of searches for parity doublets in other nuclei have been inconclusive [95, 96] or have revealed relatively widely separated parity doublets, such as those observed in ^{229}Ra [90]. Reviol and co-workers have presented evidence for low-lying parity doublets in ^{219}Th [97] and high-lying parity-doublet band structures in ^{221}Th, that are associated with the $K = 5/2$ configuration that forms the low-lying yrast structure of ^{223}Th [98].

The best examples in the $Z \approx 56$, $N \approx 88$, where the separation is about 100keV, are ^{151}Pm, ^{153}Eu and ^{155}Eu. In the last twenty years searches of odd-mass nuclei in this mass region for further examples of parity doublet bands near the ground state have been unsuccessful (e.g. [99, 100, 101, 102, 103, 104, 105, 106, 107, 108, 109]).

4. Electromagnetic transitions

In order to determine the shape of nuclei, the rotational model can be used to connect the intrinsic deformation, which is not directly observable, to the electric charge moments that arise from the non-spherical charge distribution. For quadrupole deformed nuclei, the typical experimental observables are $E2$ transition moments that are related to the matrix elements connecting differing members of rotational bands in these nuclei, and $E2$ static moments that are related to diagonal matrix elements for a single state. If the nucleus does not change its shape under rotation, both types of moments will vary with angular momentum but can be related to a constant intrinsic moment that characterizes the shape of the nucleus. For pear-shaped nuclei, there will be additionally $E1$ and $E3$ transition moments that connect rotational states having opposite parity. The $E1$ transitions can be enhanced because of the separation of the centre-of-mass and centre-of-charge, although the absolute values of the $E1$ moments are small, typically $< 10^{-2}$ single particle units. In the macroscopic-microscopic description of the $E1$ moment [110] (see also [111]), the macroscopic term has both a volume and surface contribution, while the microscopic (shell) term is a strong function of both proton and neutron number. This gives rise to large fluctuations in the value of the intrinsic dipole moment Q_1, defined using the expression

$$B(E1; I_i \rightarrow I_f) = \frac{3}{4\pi} Q_1^2 (I_i K_i 10 | I_f K_f)^2. \tag{4}$$

In the lanthanide region the macroscopic component of Q_1, $Q^{\rm macr}$, is calculated to be less than $0.03e$fm so the behaviour of Q_1 is dominated by the strongly fluctuating value of the shell contribution to Q_1, $Q^{\rm shell}$. The small experimental value of Q_1 observed for ^{146}Ba is understood in this model as arising from the cancellation between the proton and neutron contributions to $Q^{\rm shell}$ [110]. For the actinide region, the calculated values of $Q^{\rm macr}$ are much larger, typically $> 0.1e$fm. The value of $Q^{\rm shell}$ can achieve large values having the opposite sign to that of $Q^{\rm macr}$ for increasing values of N [110]. Figure 11 shows the experimental values for radium isotopes compared with different theoretical calculations. A striking feature in the plot is the small experimental value for ^{224}Ra, deduced from $B(E1)/B(E2)$ ratios [63, 113] and more recently measured absolutely [4].

This is explained naturally by the cancellation of $Q^{\rm macr}$ and $Q^{\rm shell}$ in the microscopic-macroscopic model; and also accounted for by microscopic models using, for example, HFB methods [16].

The higher order $E\lambda$ ($\lambda = 2, 3$) transition moments are collective in behaviour and generated by coherent contributions arising from the quadrupole-octupole shape. These are related to the matrix elements of the electromagnetic operators $\mathcal{M}(E_\lambda)$ and, in the rotational model, defined in terms of the intrinsic moments Q_λ

$$B(E\lambda; I_i \rightarrow I_f) = \frac{1}{(2I_i+1)}\langle I_i||\mathcal{M}(E_\lambda||I_f\rangle$$
$$= \frac{(2\lambda+1)}{16\pi}Q_\lambda^2(I_iK_i\lambda 0|I_fK_f)^2. \quad (5)$$

For a uniformly charged, spheroidal shape the Q_λ are related to the mass deformation parameters β_λ

$$Q_\lambda = \frac{3}{\sqrt{(2\lambda+1)\pi}}ZR_0^\lambda\overline{\beta_\lambda} \quad (6)$$

In this expression $R_0 = 1.2A^{\frac{1}{3}}$ and $\overline{\beta_\lambda}$ is a function of $\beta_2, \beta_3, \beta_4$... [12]. For ^{224}Ra this gives a value of 30 single particle units for $B(E3; 0^+ \rightarrow 3^-)$, if $\overline{\beta_3} = 0.1$. The E3 moment is therefore an observable that is insensitive to single-particle effects and provides the best measure of enhanced octupole correlations. For deformed nuclei it can be related to the intrinsic octupole deformation parameters [25]. Coulomb excitation is an important tool for exploring the collective behaviour of deformed nuclei that gives rise to strong enhancement of the probability of transitions between states. Traditionally, this technique has been employed by exciting targets of stable nuclei with accelerated ion beams of stable nuclei at energies below the Coulomb barrier, ensuring that the interaction is purely electromagnetic in character. Whereas $E2$, $E1$ and magnetic dipole ($M1$) transition probabilities dominate in the electromagnetic decay of nuclear states, and hence can be determined from measurements of the lifetimes of the states, $E2$ and $E3$ transition moments dominate the Coulomb excitation process allowing these moments to be determined from measurement of the cross-sections of the states, often inferred from the γ-rays that de-excite these levels.

That Coulomb excitation can be applied to the measurement of octupole bands at high spin was first demonstrated in preliminary studies of ^{148}Nd [114], in the $Z \approx 56$, $N \approx 88$ region. The results of Coulomb excitation measurements for ^{148}Nd [67, 68] and ^{150}Nd [69] are shown in figure 12. It is interesting to note that while some of the $E3$ matrix elements have values consistent with a constant intrinsic octupole moment, others have values close to zero. For example, the value of the $< 1^-||E3||4^+ >$ matrix element in ^{148,150}Nd is much smaller than the adjacent values $< 3^-||E3||0^+ >$ and $< 5^-||E3||2^+ >$. This behaviour, at least for $I < 8\hbar$, is explained in [68] in the context of the quadrupole-octupole coupling model, in which octupole phonons are weakly coupled to a deformed core [115]. In this model there will be large $E3$ transitions strengths between the I^+ states in the ground state band and the $(I+3)^-$ states formed by aligning an octopole

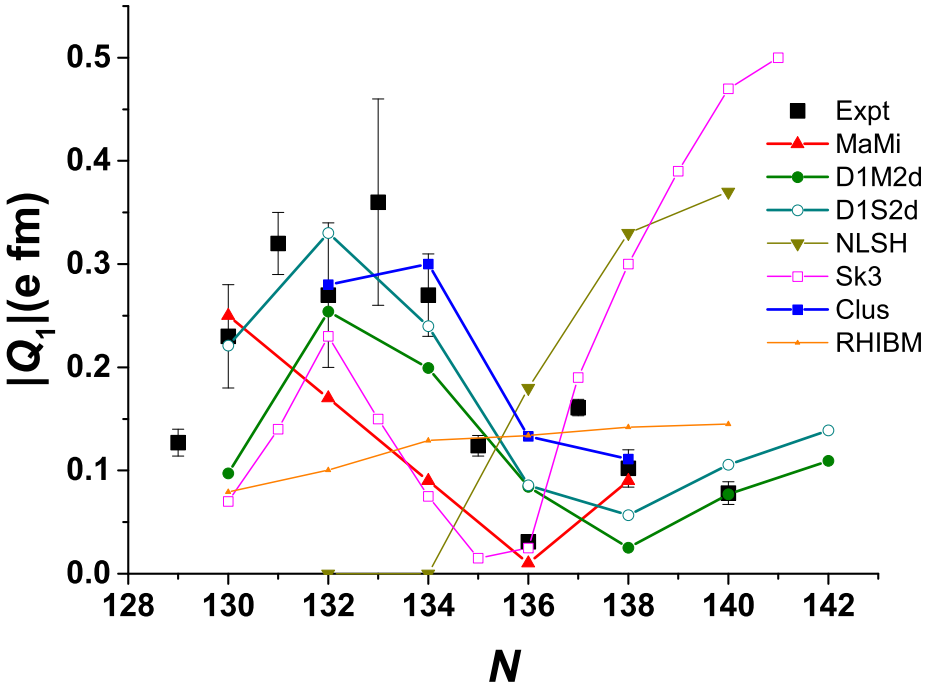

Figure 11: Measured and theoretical values of the intrinsic electric dipole moments Q_1 for radium isotopes. The measured values are for $(I+1)^- \rightarrow I^+$ transitions between low-lying states, take from [110] except for $A = 222$ [8], $A = 224$ [4], $A = 226$ [62] and $A = 228$ [4] (see also [112]). The theoretical models are: shell-corrected liquid drop models (MaMi) [3], Gogny HFB with D1M and D1S parameterizations (D1M2d and D1S2d) [27], relativistic mean field (NLSH) [17], Skyrme HF (Sk3) [24], cluster model (Clus) [21], and relativistic Hartree-Bogoliubov mapped onto *sdf* IBM (RHIBM) [28].

phonon to the positive parity states. For ^{148}Nd the $E3$ matrix elements between the octupole band and other low-lying collective bands have also been measured [68]. The appreciable enhancement of the $E3$ strength coupling the so-called beta band and the negative-parity band is consistent with a significant admixture of the octupole double-phonon vibrational mode in the wave function of the excited 0^+ band [68].

Until recently, $E3$ transition moments had been determined for only one nucleus in the $Z \approx 88$, $N \approx 134$ region, ^{226}Ra [62]. In this case the radioisotope is sufficiently long-lived to produce a macroscopic target sample. The technique has now been extended by the use of accelerated beams of radioactive nuclei such as those from the Radioactive beam EXperimental facility at ISOLDE, CERN (REX-ISOLDE [116]) and the CAlifornium Rare Ion Breeder Upgrade at the ATLAS facility, Argonne National Laboratory (CARIBU [117]). The latter facility has recently allowed the $< 3^-||E3||0^+ >$ matrix element to be measured in ^{144}Ba, in the $Z \approx 56$, $N \approx 88$ region [118]. The γ-ray spectrum obtained following bombardment of a ^{208}Pb target, is shown in the upper

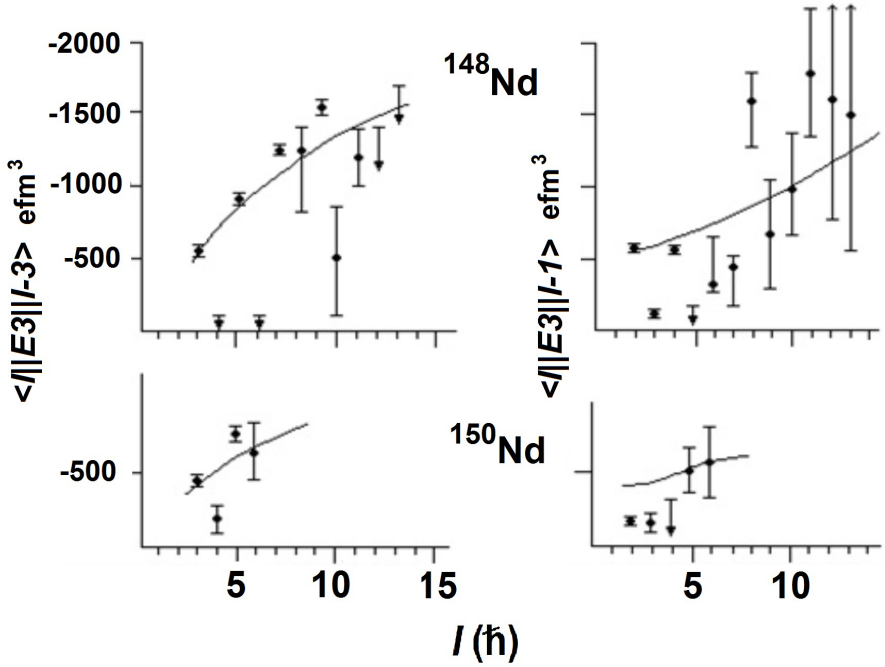

Figure 12: Measured $E3$ matrix elements for ^{148}Nd [68] and ^{150}Nd [69]. The solid lines assume that the matrix elements arise from the rotation of a fixed shape with a constant intrinsic octupole moment.

part of figure 13. In order to study octupole correlations in nuclei in the $Z \approx 88$, $N \approx 134$ region, ^{220}Rn and ^{224}Ra ions were produced by spallation in a thick uranium carbide target bombarded by protons from the CERN PS Booster. The ions were post-accelerated in REX-ISOLDE to an energy of 2.8 MeV per nucleon and bombarded various secondary targets. The γ-ray spectra obtained following the ^{224}Ra bombardment is shown in the lower part of figure 13. More details of these measurements and the GOSIA fitting procedure [119, 120] can be found in ref. [4].

Figure 14 compares the experimental values of Q_λ derived from the matrix elements connecting the lowest states for nuclei near $Z = 88$ and $N = 134$ measured by Coulomb excitation. It is striking that while the $E2$ moment increases by a factor of 6 between ^{208}Pb and ^{234}U, the $E3$ moment changes by only 50% in the entire mass region. Nevertheless, the larger Q_3 values for ^{224}Ra and ^{226}Ra indicate an enhancement in octupole collectivity that is consistent with an onset of octupole deformation in this mass region. On the other hand, ^{220}Rn has similar octupole strength to ^{208}Pb, ^{230,232}Th and ^{234}U, consistent with it being an octupole vibrator. Figure 15 shows the behaviour of Q_3 as a function of N in the lanthanide region. This quantity remains approximately constant for each isotope between $N = 82$ and $N = 88$, and then drops significantly between $N = 88$ and $N = 90$.

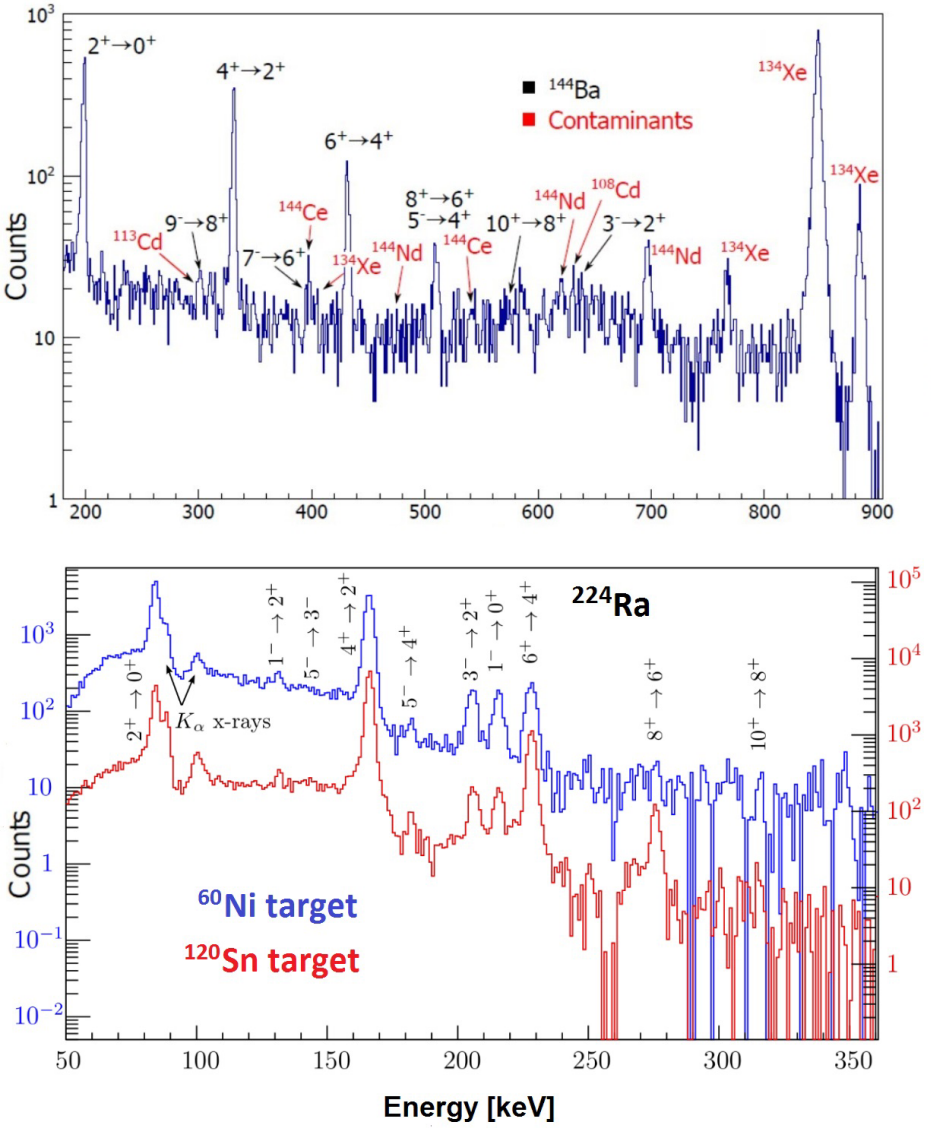

Figure 13: Upper: γ-ray spectra following the bombardment of a 1mg cm^{-2} ^{208}Pb target by a composite beam including ^{144}Ba. For details, see [118]. Lower: γ-ray spectra following the bombardment of 2mg cm^{-2} ^{60}Ni and ^{120}Sn targets by ^{224}Ra. The differences in excitation cross-section for the targets with different Z are apparent for the higher spin states. Adapted from [4].

In the case of a vibrator, as discussed earlier, the coupling of an octupole phonon to the ground state rotational band will give small values for matrix elements such as $< 1^-||E3||4^+ >$. For ^{226}Ra (and ^{224}Ra), we believe that the negative-parity states have $K^\pi = 0^-$ and result from the rotation of a rigid pear-shape. In this case the intrinsic moment derived from the measured $< 1^-||E3||4^+ >$ is similar to that derived from the value of $< 0^+||E3||3^- >$ [62], see figure 16. This figure shows the measured $E2$ and $E3$ matrix elements for ^{220}Rn, ^{224}Ra and ^{226}Ra, which are all consistent with the geometric predictions expected from a rotating, deformed distribution of electric charge. For ^{220}Rn

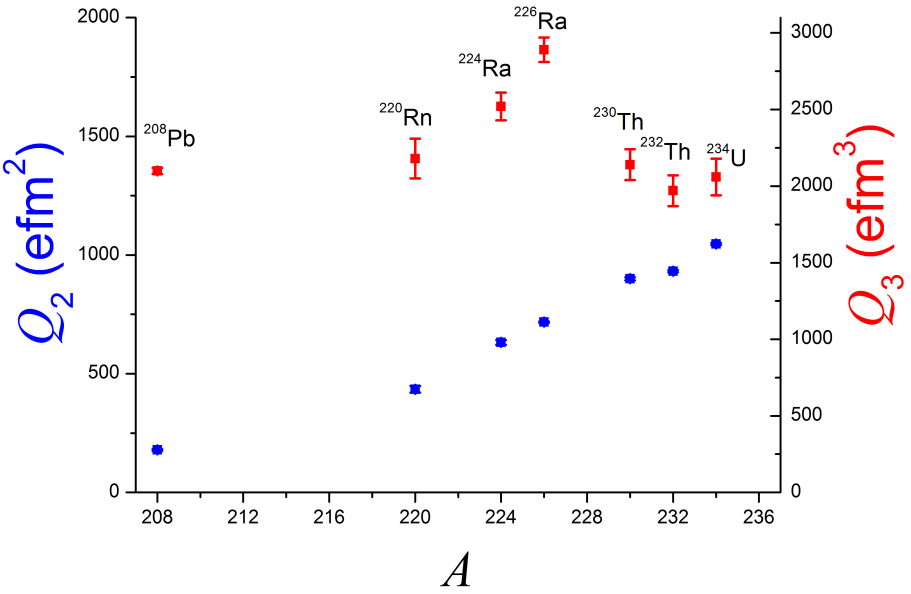

Figure 14: The systematics of measured $E2$ and $E3$ intrinsic moments Q_λ for $\lambda \to 0$ transitions in nuclei with $A > 200$. See table 2 in ref. [4] for details.

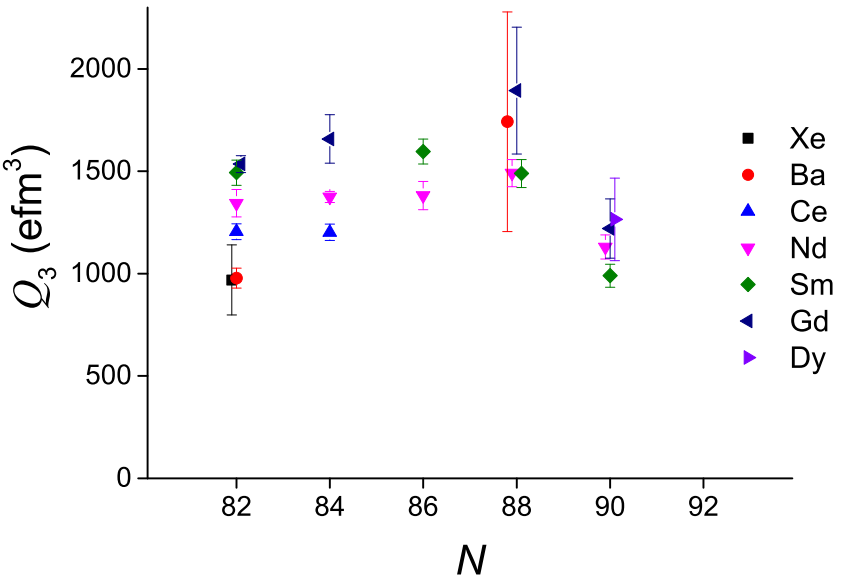

Figure 15: The systematics of measured [118, 121] $E3$ intrinsic moments Q_3 for $3^- \to 0^+$ transitions in the lanthanide region.

and ^{224}Ra the data on the electromagnetic transitions are insufficient to distinguish whether the negative-parity states arise from the projection of a quadrupole-octupole deformed shape or from an octupole oscillation of a quadrupole shape, but the behaviour

of the overall $E3$ strength combined with the energy level data support the former interpretation for ^{224}Ra and the latter for ^{220}Rn.

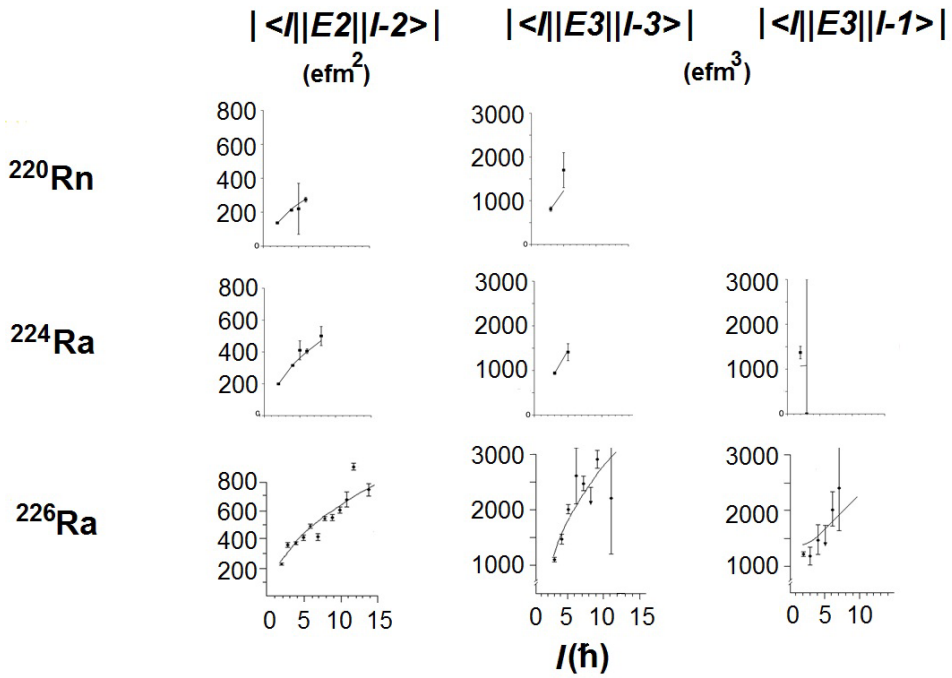

Figure 16: Measured $E2$ and $E3$ matrix elements for ^{220}Rn, ^{224}Ra [4] and ^{226}Ra [62]. The solid lines assume that the matrix elements arise from the rotation of a fixed shape with a constant intrinsic quadrupole and octupole moments.

The values of intrinsic quadrupole moments Q_2 and octupole moments Q_3 for radium isotopes, deduced from the measured transition matrix elements, are compared with various theoretical calculations in figures 17 and 18 as a function of N. For the quadrupole moments the macroscopic-microscopic and microscopic HF calculations agree quite well with each other and with the experimental data for $N > 134$. On the other hand, the calculations of the Q_3 moments diverge from each other for decreasing and increasing N away from $N = 136$. The trend of the experimental data for Q_3 is that the values increase in going from ^{224}Ra to ^{226}Ra, which contrasts with the predictions of macroscopic-microscope calculations [3], cluster model calculations [21], Gogny HFB mean-field calculations using either D1M or D1S parameterisations [27] and RHF-IBM calculations [28]. All of these models except for the cluster model predict a maximum for ^{224}Ra, although the agreement with the measurement for ^{224}Ra by itself is quite good. As can be seen, the relativistic mean field calculations [17] predict that the maximum value of Q_3 occurs for radium isotopes between $A = 226$ and 230, depending on the parameterization, and Skyrme Hartree-Fock calculations [18] predict that ^{226}Ra has the largest octupole deformation, consistent with the data. The possibility cannot completely be eliminated that there are unobserved couplings from the ground state to higher-lying 3^- states that should be added (without energy weighting) to the observed

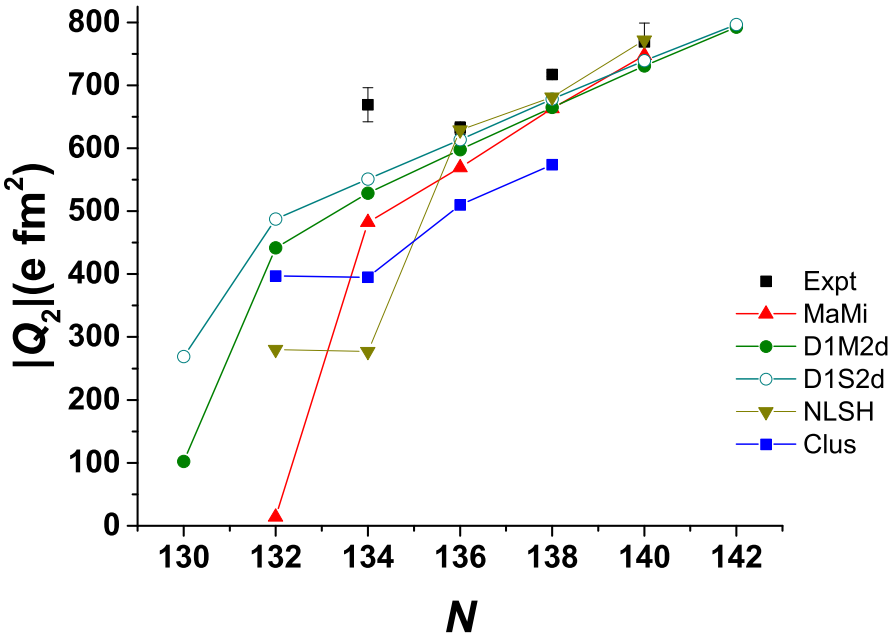

Figure 17: Values of Q_2 for low-lying transitions as a function of N for radium isotopes. Measured values for $2^+ \rightarrow 0^+$ transitions, for $A = 222$ [122], $A = 224$[4], $A = 226$ [62], and $A = 228$ [112], are compared to various theoretical models, see the caption to figure 11.

coupling to the lowest 3^- state. However, in a detailed study [68] of octupole strength in ^{148}Nd, where these states lie closer in energy to the lowest state, such couplings were not observed.

5. Future prospects

5.1. E1-E3 phase

For radium isotopes, there has been a long standing prediction [110, 111] that the sign of the $E1$ moment, Q_1, changes as the mass is increased from 222 to 226. As discussed in section 4 this arises in the macroscopic-microscopic model from the shell correction to the bulk (droplet) contribution which becomes increasingly negative as N increases. These calculations successfully reproduce the near exact cancellation for the $E1$ moment which has been observed for ^{224}Ra. As remarked earlier, microscopic models using the HFB approach also predict cancellation effects for Q_1 [16]. It is in principle possible to measure the phase of the $E1$ moment relative to the $E3$ moment for a mixed nuclear transition. In general, γ-ray decay properties depend very weakly on the $E3$ admixture, and Coulomb excitation at close nuclear distances has little dependence on the $E1$ admixture. However, the Coulex yields of low-lying negative parity states can become

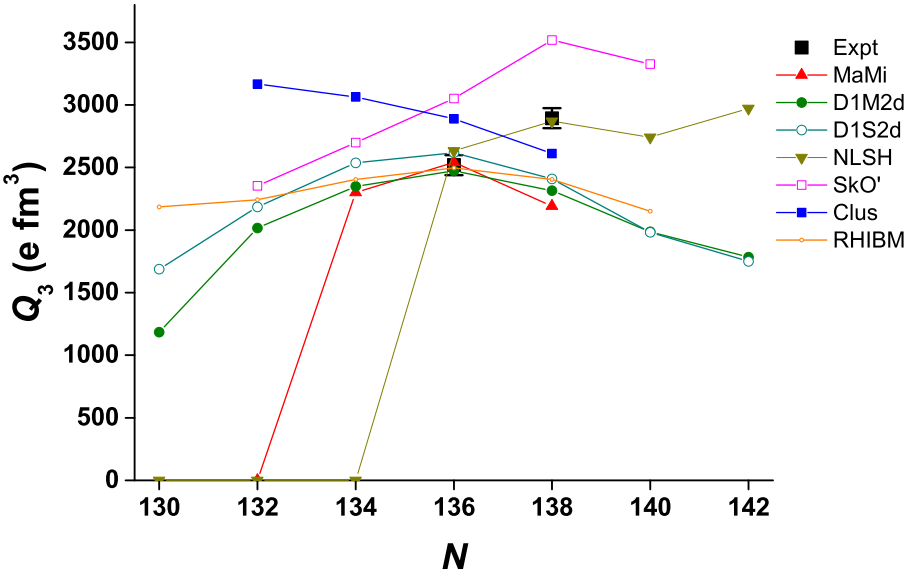

Figure 18: Values of Q_3 for low-lying transitions as a function of N for radium isotopes. Measured values for $3^- \rightarrow 0^+$ transitions, for $A = 224$ [4] and $A = 226$ [62], are compared to various theoretical models, see the caption to figure 11. In this case the Skyrme HF(SkO′) is taken from [18].

sensitive to the relative magnitudes and phase of the $E1$ and $E3$ matrix elements if the distance of closest approach is sufficiently large. This will occur at very low bombarding energies relative to the Coulomb barrier, typically 1-2 MeV per nucleon. The published data for ^{226}Ra [123] show a preference for the sign of (Q_1/Q_3) to be negative, although the data were not sufficiently accurate to establish which hypothesis for the relative phase is the correct one.

5.2. E3 moments

The recent results [4] from Coulomb excitation experiments carried out at REX-ISOLDE show that ^{220}Rn has weaker octupole collectivity than ^{224}Ra, and reveals detailed differences from various theoretical predictions. These measurements should be extended to other radioactive isotopes in the Rn and Ra chain, and experiments are planned to study $^{222-226}$Rn and ^{222,228}Ra using HIE-ISOLDE [124]. It is interesting to note that the Gogny HFB calculations [25, 26] predict that Th and U isotopes with $N = 134 - 136$, already known to exhibit the characteristics of a rigid octupole shape [8, 60], should have significantly enhanced $E3$ transition strengths (70 single-particle units), see figure 19. The predicted yields of these isotopes from the future FRIB facility [125] will be in principle be sufficient to measure the transition strengths for isotopes such as ^{226}Th and ^{228}U.

Another area for further study is to understand the structure of low-lying excited $K^\pi = 0_2^+$ bands. There is now a large body of evidence that these are not β-bands but arise from particle-hole configurations or 'pairing isomers' [75, 126]. The two-particle nature of these states can be investigated in ^{224,226}Ra and other nuclei using two-neutron transfer reactions [85] using radioactive-ion beam facilities such as HIE-ISOLDE. As discussed in the earlier sections, it has been speculated that the $K^\pi = 0_2^+$ bands in some nuclei have large double-octupole phonon components (e.g. [68, 39]). Evidence for this would come from the $E3$ matrix elements between the octupole band and the 0_2^+ band having similar strength to that between the ground-state band and the octupole band, as has been observed in ^{148}Nd [68]. These measurements should be extended to more cases, such as ^{226}Ra [86] or ^{240}Pu [39]. In particular, the observation of low-lying double-octupole phonon bands strongly coupled to the yrast negative-parity band in ^{226}Ra, explained as a condensation of octupole phonons [38], might be hard to reconcile with our current understanding that this nucleus is a prime example of a rigid pear-shape.

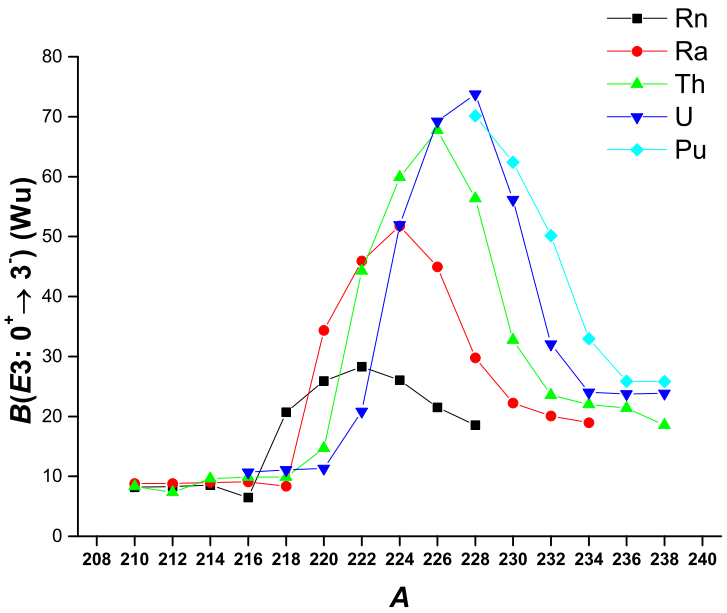

Figure 19: Theoretical values, taken from ref. [25], of $B(E3 : 0^+ \rightarrow 3^-)$ transition strengths (in single particle units) versus A for various isotopes.

5.3. Hyperdeformation

Actinide nuclei having $Z \approx 92$ and $N \approx 142$ are predicted [127] to have both super- and hyper-deformed (HD) minima lying at excitation energies ~ 3 MeV above the ground state. This arises from the large shell correction energy for this neutron number at 2:1 deformation and for both proton and neutron numbers at 3:1 deformation, superimposed

upon a Coulomb flattened liquid drop energy. The calculations were able to reproduce the measured values of the 2nd and 3rd minima excitation energies and the intermediate and outer barrier heights in ^{230,232}Th and ^{236}U. The HD minimum ($\beta_2 \approx 0.85$) predicted to lie very low in ^{230,232}U (3.3 and and 3.0 MeV respectively) has a very asymmetric bi-nuclear configuration and hence has a large octupole deformation ($\beta_3 \approx 0.6$). This minimum should become yrast at values of angular momentum of between 30 and 35 $\hbar$. At these spin values the outer barrier to fission should remain fairly robust and not too dissimilar to the value at spin zero (predicted to be ≈ 3.5 MeV). More recent calculations [128, 129] have found, however, that the depth of the third minima is much shallower than those calculated in [127], typically $\sim$ 1MeV rather than $\sim$ 4MeV.

Experimental evidence for the existence of the third minimum in neighbouring nuclei at spin zero has come from microstructure in resonances observed following (n,f), (t,pf) or (d,pf) reactions, e.g. [130, 131, 132]. If the octupole-deformed HD minimum is as deep as suggested by the earlier calculations [127] the excited states in the minimum will be populated with a measurable intensity at high spin and decay mostly by $E1$ transitions for $I \leq 25\hbar$ [133]. These will have small internal conversion for $I > 8\hbar$; the transition energy will be in the range 50 - 200 keV. The high γ-ray multiplicity ($<$ m $>\approx$ 15) of low energy transitions would provide a clear signal above the fission background which has $<$ m $>\approx$ 10 and average E_γ of 1 MeV. Attempts to detect this signal have not so far been successful [134].

5.4. Pear-shapes and EDMs

Atoms with octupole-deformed nuclei are very important in the search for permanent atomic electric-dipole moments (EDMs). The electric dipole moment must vanish if there is invariance under the parity transformation ($\mathcal{P}$) for which **r**$\rightarrow$**-r** or under the time-reversal transformation ($\mathcal{T}$) for which $t\rightarrow$-t [135]. Since the orientation of the system can be specified only by the orientation of its angular momentum, the dipole moment **d** and the angular momentum **I** must transform their signs the same way under $\mathcal{P}$ and $\mathcal{T}$ invariance. But **d** changes sign under $\mathcal{P}$ whereas **I** does not, so **d** must vanish if there is $\mathcal{P}$ symmetry. Likewise **d** does not change sign under $\mathcal{T}$ but **I** does, so **d** must vanish if there is T symmetry. Under the assumption of the $\mathcal{CPT}$ theorem, if $\mathcal{T}$ is violated then $\mathcal{CP}$ must also be violated, and the observation of a non-zero EDM at the level of contemporary experimental sensitivity would indicate $\mathcal{CP}$ violation due to physics beyond the standard model (SM). Such 'flavour-diagonal' $\mathcal{CP}$ violation has not yet been observed, although modifications of the SM that would give rise to measurable effects are strongly motivated in order to account for the observed cosmological dominance of baryons over antibaryons. In fact, experimental limits on EDMs provide important constraints on many proposed extensions to the standard model [136, 137]. For a neutral atom in its ground state, the Schiff moment S is the lowest-order observable nuclear moment. It is related to the operator corresponding to the electric-dipole distribution weighted by radius squared [138], $\hat{S}_z$, the energy splitting

of the parity doublet ΔE, and the operator corresponding to the $\mathcal{P}$ and $\mathcal{T}$ violating nucleon-nucleon interaction $\hat{V}_{\rm PT}$ in the following expression

$$S = -2\frac{I}{I+1}\frac{\left\langle \hat{S}_z \right\rangle \left\langle \hat{V}_{\rm PT} \right\rangle}{\Delta E} \tag{7}$$

where I is the ground state spin. Odd-A octupole-deformed nuclei will have enhanced nuclear Schiff moments owing to the presence of the large octupole collectivity and the occurrence of nearly degenerate parity doublets. The latter will occur naturally arise if the deformation is static [139, 138, 19, 140]. Because a $\mathcal{CP}$-violating Schiff moment induces a contribution to the atomic EDM, the sensitivity of the EDM measurement to $\mathcal{CP}$ violation over non-octupole-enhanced systems such as ^{199}Hg [137], currently providing the most stringent limit for atoms, can be improved by a large factor [19]. Essential in the interpretation of such limits is a detailed understanding of the structure of these nuclei. Experimental programmes are in place to measure EDMs in atoms of odd-A Rn and Ra isotopes in the octupole region (see for example, ref. [141, 142]) but so far there is little direct information on octupole correlations in these nuclei. The recent measurements [4] of Q_3 values in ^{220}Rn and ^{224}Ra are consistent with suggestions from the systematic studies of energy levels [66] that the even-even isotopes $^{218-222}$Rn and ^{220}Ra have vibrational behaviour while $^{222-228}$Ra have octupole-deformed character. It is concluded [4] that the parity doubling condition that leads to enhancement of the Schiff moment is unlikely to be met in ^{219,221}Rn, though more favourable Rn candidates may emerge from future studies of the low-lying structure of heavier isotopes. On the other hand ^{223,225}Ra, having parity doublets separated by ≈50 keV (ref. [2]), will have large enhancement of their Schiff moments. The measurement of the inter-band $E3$ matrix elements between the low-lying states in odd-mass nuclei using γ-ray and conversion electron spectroscopy will, however, be challenging. An alternative approach advocated [143] is to employ (d,d′) scattering (see, e.g. [144]) to populate low-lying states in odd-A nuclei via single-step excitation. In this case sufficient final-state energy resolution can be achieved for an inverse reaction such as d(^{225}Ra, d′) using a large-acceptance magnetic spectrometer [145, 146], provided that the radioactive heavy beams are cooled in a storage ring such as the TSR [147] planned to be installed at CERN.

6. Conclusions

In this topical review, the evidence for reflection asymmetric shapes in atomic nuclei has been presented. The recent developments in theoretical descriptions include a wide variety of approaches such as microscopic Hartree-Fock-Bogoliubov using both the Gogny and Skyrme family of forces, cluster and algebraic models. In general only the microscopic models (including macroscopic-microscopic approaches) are able to reproduce the behaviour of the electric dipole moments and provide global systematics that successfully map the observed regions of strong octupole correlations. Most models are able to reproduce the observed electric quadrupole moments reasonable well but there is considerable divergence in the predicted values of electric octupole moments.

Experimentally the improvements in the sensitivity of detection systems, particularly γ-ray detector arrays, have allowed wider regions of neutron-rich nuclei to be probed for octupole effects. Several isotopes of radium, thorium and uranium are shown to exhibit the hallmarks of permanent pear-shape deformation whereas the low-lying negative parity bands in most isotopes in the the lanthanide region are best described as arising from octupole vibrations.

The advent of accelerated radioactive beams has given new impetus to this field, allowing previously inaccessible nuclei to be explored using Coulomb excitation or particle transfer reactions. This will allow $E3$ strengths, a direct measure of octupole collectivity, be determined across a wide range of lanthanide and actinide nuclei. This will help pin down not only a better microscopic understanding of phenomena arising from the breaking of reflection symmetry in nuclei but also provide the understanding of the underlying nuclear structure necessary for interpreting the outcome of searches for CP-violating nuclear processes.

Acknowledgments

Support from the U.K. funding council S.T.F.C. is gratefully acknowledged. I express my appreciation to my close collaborator and colleague Graham Jones, and our PhD students who have contributed to some of the experimental work mentioned here: Nora Amzal, Dave Burrows, Nigel Clarkson, James Cocks, Ahmed El-Lawindy, Liam Gaffney, Paul Greenlees, Neil Hammond, Debbie Hawcroft, Tom Hoare, Rich Humphreys, Ray Poynter, John Smith, and Chris White. I would also like to thank Irshad Ahmad, Rafał Broda, Doug Cline, Tomek Czosnyka (dec.), Bob Cunningham, Jorrit De Boer, Luis Egido, Bogdan Fornal, Benoît Gall, Christian Günther, Rauno Julin, Sakari Juutinen, Witek Kurcewicz, Christoph Lauterbach, Georg Leander (dec.), Matti Leino, Witek Nazarewicz, Luis Robledo, Marcus Scheck, John Simpson, Frank Stephens, Waldek Urban, Bob Wadsworth, Doug Watson, Hans-Jürgen Wollersheim, Magda Zielinska, and many others with whom it has been a privilege to collaborate with.

References

[1] Reinhard P-G and Otten E W 1984 *Nucl. Phys.* A **420** 173
[2] Butler P A and Nazarewicz W 1996 *Rev. Mod. Phys.* **68** 349
[3] Nazarewicz W *et al.* 1984 *Nucl. Phys.* A **429** 269
[4] Gaffney L P *et al.* 2013 *Nature* **497** 199
[5] Neergård K and Vogel P 1970 *Nucl. Phys.* A **149** 217
[6] Bohr A and Mottelson B R 1998 *Nuclear Structure Volume II* (World Scientific)
[7] Frauendorf S 2001 *Rev. Mod. Phys.* **73** 463
[8] Cocks J F C *et al.* 1999 *Nucl. Phys.* A **645** 61
[9] Sheline R K, Jain A K, Jain K and Ragnarsson I 1989 *Phys. Lett.* B **219** 47
[10] Ahmad I and Butler P A 1993 *Annu. Rev. Nucl. Part. Sci.* **43** 71
[11] Leander G A and Sheline R K 1984 *Nucl. Phys.* A **413** 375
[12] Leander G A and Chen Y S 1988 *Phys. Rev.* C **37** 2744
[13] Möller P *et al.* 2008 *At. Data Nucl. Data Tables* **94** 758

[14] Chasman R R 1980 *Phys. Lett.* B **96** 7
[15] Bonche P, Heenen P-H, Flocard H and Vautherin D 1986 *Phys. Lett.* B **175** 387
[16] Egido J and Robledo L 1989 *Nucl. Phys.* A **494** 85
[17] Rutz K, Maruhn J A, Reinhard P-G, and Greiner W 1995 *Nucl. Phys.* A **590** 680
[18] Engel J, Bender M, Dobaczewski J, d Jesus J H and Olbratowski P 2003 *Phys. Rev.* C **68** 025501
[19] Dobaczewski J and Engel J 2005 *Phys. Rev. Lett.* **94** 232502
[20] Robledo L M and Bertsch G F 2011 *Phys. Rev.* C **84** 054302
[21] Shneidman T M *et al.* 2003 *Phys. Rev.* C **67** 014313
[22] Buck B, Merchant A C, and Perez S M 2008 *J. Phys. G: Nucl. Part. Phys.* **35** 085101
[23] Zamfir N V and Kusnezov D 2001 Phys. Rev. C **63** 054306
[24] Tsvetkov A, Kvasil J and Nazmitdinov R G 2002 *J. Phys. G: Nucl. Part. Phys.* **28** 2187
[25] Robledo L M and Bertsch G F 2012 *Phys. Rev.* C **86** 054306
[26] Robledo L M and Rodríguez-Guzmán R R 2012 *J. Phys. G: Nucl. Part. Phys.* **39** 105103
[27] Robledo L M and Butler P A 2013 *Phys. Rev.* C **88** 051302(R)
[28] Nomura K, Vretenar D, Nikšić T and Lu B-N 2014 *Phys. Rev.* C **89** 024312
[29] Li X and Dudek J 1994 *Phys. Rev.* C **94** R1250
[30] Dudek J, Gozźdź A, Schunck N and Miśkiewicz M 2002 *Phys. Rev. Lett.* **88** 252502
[31] Dudek J *et al.* 2006 *Phys. Rev. Lett.* **97** 072501
[32] Tagami S, Shimizu Y R and Dudek J 2013 *Phys. Rev.* C **87** 054306
[33] Tagami S, Shimizu Y R and Dudek J 2015 *J. Phys. G: Nucl. Part. Phys.* **42** 015106
[34] Bark R A *et al.* 2010 *Phys. Rev. Lett.* **104** 022501
[35] Jentschel M *et al.* 2010 *Phys. Rev. Lett.* **104** 222502
[36] Ntshangase S S *et al.* 2010 *Phys. Rev.* C **82** 041305(R)
[37] Reviol W *et al.* 2006 *Phys. Rev.* C **74** 044305
[38] Frauendorf S 2008 *Phys. Rev.* C **77** 021304
[39] Wang X *et al.* 2009 *Phys. Rev. Lett.* **102** 122501
[40] Minkov N *et al.* 2006 *J. Phys. G: Nucl. Part. Phys.* **32** 497
[41] Jolos R V, Minkov N and Scheid W 2005 *Phys. Rev.* C **72** 064312
[42] Jolos R V and von Brentano P 2015 *Phys. Rev.* C **92** 044318
[43] Walker P M and Minkov N 2010 *Phys. Lett.* B **694** 119
[44] Minkov N and Walker P M 2012 *Eur. Phys. J* A **48** 80
[45] Minkov N and Walker P M 2014 *Phys. Scr.* **89** 054021
[46] Liu H L and Xu F R 2013 *Phys. Rev.* C **87** 067304
[47] Iachello F 2001 *Phys. Rev. Lett.* **87** 052502
[48] Bizzeti P G and Bizzeti-Sona A M 2004 *Phys. Rev.* C **70** 064319
[49] Bizzeti P G and Bizzeti-Sona A M 2008 *Phys. Rev.* C **77** 024320
[50] Bizzeti P G and Bizzeti-Sona A M 2013 *Phys. Rev.* C **88** 011305(R)
[51] Bizzeti P G and Bizzeti-Sona A M 2010 *Phys. Rev.* C **81** 034320
[52] Cottle P D and Zamfir N V 1998 *Phys. Rev.* C **58** 1500
[53] Otsuka T and Sugita M 1988 *Phys. Lett.* B **209** 140
[54] Daley H and Iachello F 1983 *Phys. Lett.* B **131** 281
[55] Asaro F, Stephens F, Jr. and Perlman I 1953 *Phys. Rev.* **92** 1495
[56] Stephens F S, Jr., Asaro F and Perlman I 1955 *Phys. Rev.* **100** 1543
[57] Ward D *et al.* 1983 *Nucl. Phys.* A **406** 591
[58] Burrows J D *et al.* 1984 *J. Phys. G: Nucl. Part. Phys.* **10** 1449
[59] Dahlinger M *et al.* 1988 *Nucl. Phys.* A **484** 337
[60] Greenlees P T *et al.* 1998 *J. Phys. G: Nucl. Part. Phys.* **24** L63
[61] Humphreys R D *et al.* 2004 *Phys. Rev.* C **69** 064324
[62] Wollersheim H J *et al.* 1993 *Nucl. Phys.* A **556** 261
[63] Poynter R J *et al.* 1989 *Phys. Lett.* B **232** 447
[64] Smith J F *et al.* 1995 *Phys. Rev. Lett.* **75** 1050

[65] Broda R *et al.* 1990 *Phys. Lett.* B **251** 245
[66] Cocks J F C *et al.* 1997 *Phys. Rev. Lett.* **78** 2920
[67] Ibbotson R W *et al.* 1993 *Phys. Rev. Lett.* **71** 1990
[68] Ibbotson R W *et al.* 1997 *Nucl. Phys.* A **619** 213
[69] Clarkson N 1992 Ph.D. thesis (University of Liverpool)
[70] Phillips W R *et al.* 1986 *Phys. Rev. Lett.* **57** 3257
[71] Wilhelmy J B *et al.* 1972 *Phys. Rev.* C **5** 2041
[72] Hamilton J H *et al.* 1995 *Prog. Part. Nucl. Phys.* **35** 635
[73] Nazarewicz W, Leander G A and Dudek J 1987 *Nucl. Phys.* A **467** 437
[74] Wiedenhöver I *et al.* 1999 *Phys. Rev. Lett.* **83** 2143
[75] Sharpey-Schafer J F *et al.* 2016 *Physica Scripta* to be published
[76] Garrote E, Egido JL and Robledo LM 1998 *Phys. Rev. Lett.* **80** 4398
[77] Urban W *et al.* 1997 *Nucl. Phys.* A **613** 107
[78] Urban W *et al.* 2001 *Acta Phys.Polon.* B **32** 2527
[79] Urban W *et al.* 2003 *Eur. Phys. J.* A **16** 303
[80] Chen YJ *et al.* 2006 *Phys. Rev.* C **73** 054316
[81] Zhu S J *et al.* 2012 *Phys. Rev.* C **85** 014330
[82] Li H J *et al.* 2012 *Phys. Rev.* C **86** 067302
[83] Garrett P E *et al.* 2005 *J. Phys. G: Nucl. Part. Phys.* **31** S1855
[84] Zhu S *et al.* 2010 *Phys. Rev.* C **81** 041306(R)
[85] Spieker M *et al.* 2013 *Phys. Rev.* C **88** 041303(R)
[86] Ackermann B *et al.* 1996 *Z. Phys.* A **355** 151
[87] Weber T, Gröger J, Günther C and de Boer J 1998 *Eur. Phys. J.* A **1** 39
[88] Stephens F S, Jr., Asaro F, and Perlman I 1954 *Phys. Rev.* **96** 1568
[89] Poynter R J *et al.* 1989 *J. Phys. G: Nucl. Part. Phys.* **15** 449
[90] Fraile L M *et al.* 1999 *Nucl. Phys.* A **657** 355
[91] Hoare T H *et al.* 1991 *J. Phys. G: Nucl. Part. Phys.* **17** 145
[92] Kalaninová Z *et al.* 2015 *Phys. Rev.* C **92** 014321
[93] Müller U *et al.* 1997 *Phys. Rev.* C **55** 2267
[94] Hammond N J *et al.* 2002 *Phys. Rev.* C **65** 064315
[95] Burke D G *et al.* 1997 *Nucl. Phys.* A **612** 91
[96] Gulda K *et al.* 2002 *Nucl. Phys.* A **703** 45
[97] Reviol W 2009 *Phys. Rev.* C **80** 011304(R)
[98] Reviol W 2014 *Phys. Rev.* C **90** 044318
[99] Jones M A *et al.* 1996 *Nucl. Phys.* A **605** 133
[100] Jones M A *et al.* 1996 *Nucl. Phys.* A **609** 201
[101] Urban W *et al.* 1996 *Phys. Rev.* C **54** 945
[102] Zhu S J *et al.* 1997 *J. Phys. G: Nucl. Phys.* **23** L77
[103] Zhu S J *et al.* 1999 *Phys. Rev.* C **59** 1316
[104] Luo Y X *et al.* 2009 *Nucl. Phys.* A **818** 121
[105] Luo Y X *et al.* 2010 *Nucl. Phys.* A **838** 1
[106] Urban W *et al.* 2012 *Phys. Rev.* C **86** 017301
[107] Rząca-Urban T *et al.* 2012 *Phys. Rev.* C **86** 044324
[108] Rząca-Urban T *et al.* 2013 *Phys. Rev.* C **87** 031305(R)
[109] Ruchowska E *et al.* 2015 *Phys. Rev.* C **92** 034328
[110] Butler P A and Nazarewicz W 1991 *Nucl. Phys.* A **533** 249
[111] Leander G *et al.* 1986 *Nucl. Phys.* A **453** 58
[112] Gulda K *et al.* 1998 *Nucl. Phys.* A **636** 28
[113] Marten-Tölle M *et al.* 1990 *Z. Phys.* A **336** 27
[114] Butler P A 1989 *Heavy Ions in Nuclear and Atomic Physics*, editors Z. Wilhelmi and G. Szeflińska (Adam Hilger) p. 295

[115] Nomura M 1975 *Phys. Lett.* B **55** 357
[116] Voulot D *et al.* 2008 *Nucl. Instrum. Methods* B **266** 4103
[117] Savard G *et al.* 2008 *Nucl. Instrum. Methods* B **266** 4086
[118] Bucher B *et al.* 2016 *Phys. Rev. Lett.* **116** 112503
[119] Czosnyka T, Cline D and Wu C Y 1983 *Bull. Am. Phys. Soc.* **28** 745
[120] Cline D 1993 *Nucl. Phys.* A **557** 615
[121] Kibédi T and Spear RH 2002 *Atom. Data Nucl. Data Tables* **80** 35
[122] Singh S, Jain A K and Jagdish K T 2011 *Nucl. Data Sheets* **112** 2851
[123] Amzal N *et al.* 2004 *Nucl. Phys.* A **374** 465
[124] Lindroos M, Butler P A, Huyse M and Riisager K 2008 *Nucl. Instrum. Methods* B **266** 4687
[125] Wrede C 2015 *EPJ Web Conf.* **93** 07001
[126] Garrett P E 2001 *J. Phys. G: Nucl. Part. Phys.* **27** R1
[127] Ćwiok S *et al.* 1994 *Phys. Lett.* B **322** 304
[128] Kowal M and Skalski J 2012 *Phys. Rev.* C **85** 061302(R)
[129] Ichikawa T, Möller P and Sierk A J 2013 *Phys. Rev.* C **87** 054326
[130] Blons J 1989 *Nucl. Phys.* A **502** 121c
[131] Krasznahorkay A *et al.* 1998 *Phys. Rev. Lett.* **80** 2073
[132] Nenoff N *et al.* 2007 *Eur. Phys. J.* A **32** 165
[133] Skalski J 1994 *Phys. Rev.* C **49** 2011
[134] Hawcroft D *et al.* 1999 *Act. Phys. Pol.* B **30** 789
[135] Ramsey N F 1990 *Annu. Rev. Nucl. Part. Sci.* **40** 1
[136] Pospelov M and Ritz A 2005 *Ann. Phys.* **318** 119
[137] Griffith W C *et al.* 2009 *Phys. Rev. Lett.* **102** 101601
[138] Spevak V, Auerbach N and Flambaum V V 1997 *Phys. Rev.* C **56** 1357
[139] Haxton W C and Henley E M 1983 *Phys. Rev. Lett.* **51** 1937
[140] Ellis J, Lee J and Pilaftsis A 2011 *J. High Energy Phys.* doi:10.1007/JHEP02(2011)045
[141] Guest J R *et al.* 2007 *Phys. Rev. Lett.* **98** 093001
[142] Wilschut H W *et al.* 2010 *Nucl. Phys.* A **844** 143c
[143] Butler P A *et al.* 2016 *Nucl. Instrum. Methods* B doi:10.1016/j.nimb.2015.12.006
[144] Thorsteinsen T F, Nybø K and Løvhøiden G 1990 *Physica Scripta* **42** 141
[145] Wuosmaa A H *et al.* 2007 *Nucl. Instrum. Methods* A **580** 1290
[146] Lighthall J C *et al.* 2010 *Nucl. Instrum. Methods* A **622** 97
[147] Grieser M *et al.* 2012 *Eur. Phys. J. Special Topics* **207** 1